

A New Partition Strategy for the Optimization Algorithm DIRECT

Hong Zhu and David B. Bogy

Computer Mechanics Laboratory
Department of Mechanical Engineering
University of California at Berkeley
Berkeley, CA 94720

ABSTRACT

This report investigates a new partition strategy for the DIRECT algorithm, which is locally biased. Several numerical experiments show that the new partition strategy can significantly increase the convergence rate for the DIRECT algorithm and its variations. It is then applied to slider ABS optimization and the improvements in the design process are discussed.

1. INTRODUCTION

The DIRECT algorithm is a global deterministic optimization algorithm that is guaranteed to converge rapidly (Jones et al., 1993). It can generally find the global minimum points very quickly as compared with other algorithms such as Simulated Annealing and Genetic Algorithm (Jones et al., 1993; Gablonsky, 1998, 2001).

We presented the details of the DIRECT algorithm, the results of numerical experiments, and its application to slider Air Bearing Surface (ABS) optimization in CML technical report [01-003](#). The results verified the very fast convergence rate of the DIRECT algorithm and showed that it is suitable for slider ABS optimization.

We also presented three locally biased variations of the standard DIRECT algorithm in CML technical report [01-007](#). These investigations showed that the three locally biased variations of the DIRECT algorithm generally have higher convergence rates than does the standard DIRECT algorithm. The variations perform especially well in some situations and they may dramatically reduce the time needed to find the global minimum points.

In the CML technical report [01-013](#) we discussed two modifications to the standard DIRECT algorithm: one to handle tolerances (minimum side lengths) and one to deal with hidden constraints. These two modifications of the DIRECT algorithm improve its efficiency and make it more flexible.

In this report, we propose a new partition strategy for the DIRECT algorithm and its variations. After presenting the new partition strategy, we conduct some numerical experiments and then discuss the results. We apply the new partition strategy to slider ABS optimization, present some results and draw our conclusions.

2. *PARTITION STRATEGY*

2.1 Review of the standard partition strategy

The standard partition strategy of the DIRECT algorithm is defined as follows:

Any potentially optimal box (either a hyper-cube or a hyper-rectangle) is only partitioned along its longest sides or dimensions. Assume m_0 is the center point of the box, δ is 1/3 of the longest side length of the box and e_i is the i^{th} Euclidean base-vector for the dimension of longest side. Then we generate sample points at $m_0 \pm \delta e_i$. Define $s_i = \min \{ f(m_0 - \delta e_i), f(m_0 + \delta e_i) \}$, and partition in the order given by s_j , starting with the smallest s_j . In this way, the box is first partitioned along the direction with the smallest s_i , and then the remaining field is partitioned along the direction of the second smallest s_i , and so on until the partition is done for all the directions with the longest side.

To demonstrate the partition strategy, we consider a 2-D test function defined as:

$$F(x_1, x_2) = (x_1 - 0.4)^2 + (x_2 - 0.2)^2 \quad \text{where } x_1, x_2 \in [0, 1].$$

Figures 1A ~ 1D show the initial state and the first 3 iterations of the DIRECT algorithm (with the standard partition strategy) for this 2-D case. In these figures, the unit square is the search space. The shadowed areas are the potentially optimal boxes (can be squares or rectangles) just partitioned. The dots represent the center points of the boxes and the circular dot shows the sample point with the smallest function value. The numbers under those dots are the function values at those sample points.

From Fig. 1B we see that

$$s_1 = \min \{0.144, 0.278\} = 0.144$$

$$s_2 = \min \{0.0111, 0.411\} = 0.0111$$

So the x_2 direction gets partitioned first, and then the x_1 direction gets partitioned.

From Fig. 1C we see that the rectangles were only partitioned along their longest side.

2.1 New partition strategy

Here we propose a new partition strategy for DIRECT as follows:

Any potentially optimal box (either a hyper-cube or a hyper-rectangle) is partitioned only along its dimensions with the longest side length. Suppose n dimensions of a N -dimensional potentially optimal box ($n \leq N$) have the longest side length. Assume m_0 is the center point of the box, δ is 1/3 of the longest side length of the box and e_i is the i^{th} Euclidean base-vector for the dimension with the longest side, where $i = 1, 2, \dots, n$, then we partition the

box in n steps. There are only two sample points generated at each step. At the i^{th} step, we generate the sample points at $m_{i-1} \pm \delta e_i$ and partition the box containing m_{i-1} evenly along the direction i into three boxes with the three sample points m_{i-1} , $m_{i-1} \pm \delta e_i$ as the center points. We define m_i as the center point of a box which will be used to generate new sample points and be partitioned at step $i+1$ as $f(m_i) = \min \{f(m_{i-1} - \delta e_i), f(m_{i-1}), f(m_{i-1} + \delta e_i)\}$. The partition process is repeated until the partition is done for all the directions with the longest side.

From the above description it is apparent that the standard partition strategy always generates all the sample points first. After that the next partition is carried out according to the evaluation results of the sample points. The new partition strategy presented here only generates two sample points at a time along a certain direction and then conducts the partition. The partitioned box containing the minimum point is then chosen to generate new sample points subsequently. It follows that the new partition strategy focuses more on local minimum points and it is therefore locally biased as compared with the standard partition strategy.

Figures 2A ~ 2D show the initial state and the first 3 iterations of the DIRECT algorithm using the new partition strategy for the same 2-D case just mentioned.

In Fig. 2B, two sample points were first generated along the x_1 direction and the search space was partitioned evenly into three rectangular boxes. Since $\min \{0.144, 0.1, 0.278\} = 0.1$, the box containing the original midpoint was then chosen to be partitioned

along the x_2 direction. After two more sample points were generated around it along the x_2 direction, the box was again partitioned evenly into three square boxes.

In Fig. 2C, two boxes (a square box and a rectangular box) were chosen to be the potentially optimal boxes and subsequently partitioned. For the square box, since we have $\min \{0.00123, 0.0111, 0.0457\} = 0.00123$ after two sample points were generated along the x_1 direction, the box containing the sample point of minimum value 0.00123 was then chosen to be partitioned along the x_2 direction subsequently. From Fig. 2C we also see that the rectangular box was only partitioned along its longest side.

3. *NUMERICAL EXPERIMENTS*

To investigate the performance difference between the new partition strategy and the standard one, we will conduct some numerical experiments in this section. For each test function, we use 4 versions of the DIRECT algorithm:

DIRECT : DIRECT algorithm with the standard partition strategy

DIRECT + : DIRECT algorithm with the new partition strategy

DIRECT-III : Locally biased variation of the DIRECT algorithm with standard partition strategy

DIRECT-III + : Locally biased variation of the DIRECT algorithm with new partition strategy

The “+” sign represents the new partition strategy. DIRECT-III is a locally biased variation of the DIRECT algorithm and it has the highest convergence rate among DIRECT and its three locally biased variations. More details of DIRECT-III can be found in CML technical report [01-007](#).

3.1 Test functions with one global minimum point

3.1.1 Easy test function cases

The easy functions used here include 2-D, 3-D, 5-D, 10-D, 20-D and 40-D quadratic functions and a 2-D Easom function. These functions are monotonic and have only one global and local minimum point. The minimum values of these functions are 0. The quadratic test functions are defined as follows:

$$2\text{-D: } F(x_1, x_2) = (x_1 - 0.4)^2 + (x_2 - 0.2)^2.$$

$$3\text{-D: } F(x_1, x_2, x_3) = (x_1 - 0.2)^2 + (x_2 - 0.3)^2 + (x_3 - 0.4)^2.$$

$$5\text{-D: } F(x_1, x_2, x_3, x_4, x_5) = (x_1 - 0.1)^2 + (x_2 - 0.3)^2 + (x_3 - 0.5)^2 + \\ (x_4 - 0.7)^2 + (x_5 - 0.9)^2.$$

$$10\text{-D: } F(x_1, x_2, x_3, x_4, x_5, x_6, x_7, x_8, x_9, x_{10}) = (x_1 - 0.1)^2 + (x_2 - 0.2)^2 + (x_3 - 0.3)^2 + \\ (x_4 - 0.4)^2 + (x_5 - 0.5)^2 + (x_6 - 0.6)^2 + \\ (x_7 - 0.7)^2 + (x_8 - 0.8)^2 + (x_9 - 0.9)^2 + \\ (x_{10} - 1.0)^2.$$

$$\begin{aligned}
20\text{-D: } F(x_1, x_2, x_3, x_4, x_5, x_6, x_7, x_8, x_9, x_{10}, x_{11}, x_{12}, x_{13}, x_{14}, x_{15}, x_{16}, x_{17}, x_{18}, x_{19}, x_{20}) = \\
& (x_1 - 0.05)^2 + (x_2 - 0.1)^2 + (x_3 - 0.15)^2 + (x_4 - 0.2)^2 + \\
& (x_5 - 0.25)^2 + (x_6 - 0.3)^2 + (x_7 - 0.35)^2 + (x_8 - 0.4)^2 + \\
& (x_9 - 0.45)^2 + (x_{10} - 0.5)^2 + (x_{11} - 0.55)^2 + (x_{12} - 0.6)^2 + \\
& (x_{13} - 0.65)^2 + (x_{14} - 0.7)^2 + (x_{15} - 0.75)^2 + (x_{16} - 0.8)^2 + \\
& (x_{17} - 0.85)^2 + (x_{18} - 0.9)^2 + (x_{19} - 0.95)^2 + (x_{20} - 1.0)^2.
\end{aligned}$$

$$\begin{aligned}
40\text{-D: } F(x_1, x_2, x_3, x_4, x_5, x_6, x_7, x_8, x_9, x_{10}, x_{11}, x_{12}, x_{13}, x_{14}, x_{15}, x_{16}, x_{17}, x_{18}, x_{19}, x_{20}, x_{21}, \\
x_{22}, x_{23}, x_{24}, x_{25}, x_{26}, x_{27}, x_{28}, x_{29}, x_{30}, x_{31}, x_{32}, x_{33}, x_{34}, x_{35}, x_{36}, x_{37}, x_{38}, x_{39}, x_{40}) = \\
& (x_1 - 0.025)^2 + (x_2 - 0.05)^2 + (x_3 - 0.075)^2 + (x_4 - 0.1)^2 + (x_5 - 0.125)^2 + \\
& (x_6 - 0.15)^2 + (x_7 - 0.175)^2 + (x_8 - 0.2)^2 + (x_9 - 0.225)^2 + (x_{10} - 0.25)^2 + \\
& (x_{11} - 0.275)^2 + (x_{12} - 0.3)^2 + (x_{13} - 0.325)^2 + (x_{14} - 0.35)^2 + (x_{15} - 0.375)^2 + \\
& (x_{16} - 0.4)^2 + (x_{17} - 0.425)^2 + (x_{18} - 0.45)^2 + (x_{19} - 0.475)^2 + (x_{20} - 0.5)^2 + \\
& (x_{21} - 0.525)^2 + (x_{22} - 0.55)^2 + (x_{23} - 0.575)^2 + (x_{24} - 0.6)^2 + (x_{25} - 0.625)^2 + \\
& (x_{26} - 0.65)^2 + (x_{27} - 0.675)^2 + (x_{28} - 0.7)^2 + (x_{29} - 0.725)^2 + (x_{30} - 0.75)^2 + \\
& (x_{31} - 0.775)^2 + (x_{32} - 0.8)^2 + (x_{33} - 0.825)^2 + (x_{34} - 0.85)^2 + (x_{35} - 0.875)^2 + \\
& (x_{36} - 0.9)^2 + (x_{37} - 0.925)^2 + (x_{38} - 0.95)^2 + (x_{39} - 0.975)^2 + (x_{40} - 1.0)^2.
\end{aligned}$$

For these cases, $x_i \in [0, 1]$, $i = 1, \dots, 40$, $f_{min} = 0$.

Figures 3 ~ 8 show the convergence comparison among DIRECT, DIRECT+, DIRECT-III and DIRECT-III + for the 2-D, 3-D, 5-D, 10-D, 20-D and 40-D quadratic test functions, respectively. In all these cases, the new partition strategy results in a higher convergence rate than does the standard partition strategy with respect to either DIRECT or

DIRECT-III algorithm. Especially, when the new strategy is applied to DIRECT-III, the resulting DIRECT-III + has the highest convergence rate among the four algorithms. As the dimensions of a problem increase, the search space becomes much larger, and the difference among the convergence rates of those four algorithms becomes more obvious. We see from [Figs. 6~8](#) that for the 10-D, 20-D and 40-D cases, DIRECT-III + shows superior performance.

The 2-D Easom function is defined as:

$$F(x_1, x_2) = 1 - \cos(x_1) \cdot \cos(x_2) \cdot e^{-((x_1-\pi)^2 + (x_2-\pi)^2)}, \text{ where } x_1, x_2 \in [0, 5].$$

It has a minimum value 0 at (π, π) .

The contour lines and the surface shape of the normalized Easom function are shown in [Figs. 9](#) and [10](#), respectively. In [Fig. 9](#) the round dot denotes the location of the global minimum point. The convergence comparison showed by [Fig. 11](#) exhibits the same trend as the results from the quadratic function cases.

[Figures 12 ~ 15](#) show the optimization results obtained by using DIRECT, DIRECT +, DIRECT-III and DIRECT-III + respectively. The tiny dots represent the sample points generated and the circular dots represent the best points found by the algorithms. From [Figs. 12 ~ 15](#) it's clear that all four algorithms converge to the global minimum point. Comparing [Figs. 12](#) and [14](#), we see that, since DIRECT-III is a locally biased variation and it focuses much more on a local search than DIRECT, it leaves a relatively larger unexplored area. Since the new partition strategy focuses more on the local search than does the standard

partition strategy, by applying it to DIRECT and DIRECT-III, DIRECT becomes locally biased and DIRECT-III becomes even more locally biased. Therefore, results of DIRECT + and DIRECT-III + show relatively larger unexplored areas than those of DIRECT and DIRECT-III, respectively.

3.1.2 Tough test function cases

The so-called “tough” functions are the ones whose global minima are difficult for the optimization technique to find. This is mostly caused by either multiple local minima or a wide “flat” area around the global minimum point. These features make the optimization difficult since it’s easy for the process to get trapped at a local minimum, or, conversely, because it’s hard to reach the global minimum point.

We investigated the Goldstein Price function, Rastrigin function, Ackley’s Path function and Rosen Brock functions in this section. They are defined as following:

Goldstein Price function:

$$f(x_1, x_2) = [1 + (x_1 + x_2 + 1)^2 \cdot (19 - 14x_1 + 3x_1^2 - 14x_2 + 6x_1x_2 + 3x_2^2)] \cdot [30 + (2x_1 - 3x_2)^2 \cdot (18 - 32x_1 + 12x_1^2 + 48x_2 - 36x_1x_2 + 27x_2^2)] - 3,$$

where $x_1, x_2 \in [-2, 2]$, $f_{min} = f(0, -1) = 0$.

Rastrigin function:

$$f(x_1, x_2) = 20 + (x_1^2 - 10 \cos(2\pi x_1)) + (x_2^2 - 10 \cos(2\pi x_2)),$$

where $x_1, x_2 \in [-4, 6]$, $f_{min} = f(0, 0) = 0$.

Ackley's Path function:

$$f(x_1, x_2) = -20 \cdot e^{(-0.2 \cdot \sqrt{0.5 \cdot (x_1^2 + x_2^2)})} - e^{(0.5 \cdot (\cos(2\pi x_1) + \cos(2\pi x_2)))} + 20 + e,$$

where $x_1, x_2 \in [-4, 6]$, $f_{min} = f(0, 0) = 0$.

2-D, 3-D and 4-D Rosen Brock functions:

$$f(x_1, \dots, x_n) = \sum_{i=1}^{n-1} (100 \cdot (x_{i+1} - x_i)^2 + (1 - x_i)^2),$$

where $n=2, 3, 4$, $x_1 \dots x_n \in [-2.048, 2.048]$, $f_{min} = f(1, \dots, 1) = 0$.

Figures 16 and 17 show the contour lines and the surface shape of the normalized Goldstein Price function, respectively. The round dot in Fig. 16 denotes the location of the global minimum point. We see that the global minimum point is located in a wide flat valley, which is why it is difficult for the optimization algorithm to find the global minimum.

Figure 18 shows the convergence comparison among DIRECT, DIRECT+, DIRECT-III and DIRECT-III + for the 2-D Goldstein Price function case. We see that the new partition strategy results in a higher convergence rate than does the standard partition strategy with respect to either DIRECT or DIRECT-III algorithm. And DIRECT-III + has the highest convergence rate among the four algorithms.

Figures 19 ~ 20 show the optimization results obtained by using DIRECT, DIRECT +, DIRECT-III and DIRECT-III + respectively. Again, the tiny dots represent the sample points generated and the circular dots represent the best points found by the algorithms. We see that all four algorithms converge to the global minimum point. However, since the new partition strategy focuses more on the local search than does the standard partition strategy and DIRECT-III is a strongly locally biased variation of DIRECT, results of DIRECT-III + leave relatively the largest unexplored areas in the square search space than the other three algorithms.

The Rastrigin function is a highly multimode function with lots of local minima. Figures 23 and 24 show the contour lines and the surface shape of the normalized Rastrigin function, respectively. The convergence comparison in Fig. 25 shows that in the early stage, which is before 350 function evaluations in this case, DIRECT + shows the highest convergence rate. But after that, once DIRECT-III + got close to the global minimum, it exhibits much higher convergence rate than does DIRECT +. Figures 26 ~ 29 show the optimization results obtained by using DIRECT, DIRECT +, DIRECT-III and DIRECT-III + respectively after 400 function evaluations. All four algorithms converge to the global minimum point.

Ackley's Path function is also a widely used multimode test function. Figures 30 and 31 show the contour lines and the surface shape of the normalized Ackley's Path function, respectively. Figure 32 shows the convergence comparison after 200 function evaluations. DIRECT-III + shows the highest convergence rate among the four algorithms. Figures 33 ~

36 show the optimization results obtained by using DIRECT, DIRECT +, DIRECT-III and DIRECT-III + respectively. Again, all four algorithms converge to the global minimum point.

The Rosen Brock function, also known as the Banana function, provides a classic optimization problem. The global minimum point is inside a long, narrow, parabolic shaped flat valley. To find the valley is trivial. However, convergence to the global minimum is very difficult and hence this problem has been repeatedly used in assess the performance of optimization algorithms. We investigate 2-D, 3-D and 4-D Rosen Brock functions here.

Figures 37 and 38 show the contour lines and the surface shape of the normalized 2-D Rosen Brock function, respectively. Figure 39 shows the convergence comparison after 500 function evaluations. DIRECT-III + shows the highest convergence rate among the four algorithms. Figures 40 ~ 43 show the optimization results obtained by using DIRECT, DIRECT +, DIRECT-III and DIRECT-III + respectively. We see that all four algorithms converge to the global minimum point and the sample points generated in each case clearly demonstrate the “banana” shaped valley of the Rosen Brock function.

Figures 44 and 45 show the convergence comparison for the 3-D and 4-D Rosen Brock functions, respectively. The 3-D case shows the similar convergence pattern as in the 2-D case. In the 4-D case, after DIRECT-III + approached the global minimum after 1200 function evaluations, it shows higher convergence rate than DIRECT +.

3.2 Test functions with multiple global minimum points

3.2.1 Easy test function cases

We consider two test functions. The first test function is called “six-hump” function, defined as:

$$F(x_1, x_2) = 4x_1^2 - 2.1x_1^4 + (1/3)x_1^6 + x_1x_2 - 4x_2^2 + 4x_2^4,$$

where $x_1 \in [-2, 2]$, $x_2 \in [-1, 1]$. This function has two global minimum points and 4 other local minimum points. If we normalize the range of variables x_1 and x_2 into $[0, 1]$, then its global minimum points are (0.52246, 0.14367) and (0.47754, 0.85633) and its global minimum is -1.03163.

The contour lines and the surface shape of the six-hump function are shown in [Figs. 46](#) and [47](#). The round dots in [Fig. 46](#) represent the global minimum points. We can clearly discern the six “humps” from these two figures. [Figures 48 ~ 51](#) show the optimization results obtained by using DIRECT, DIRECT +, DIRECT-III and DIRECT-III +, respectively. The tiny dots represent the sample points in the center of the boxes. The centers of the circles represent the location of the global minimum points. We can observe the strongly locally biased property of DIRECT-III and DIRECT-III + by looking at their large unexplored areas.

It’s clear from [Figs. 48 ~ 51](#) that sample points cluster around the two global minimum points for all four algorithms. Thus, all algorithms found the two global minimum points.

The second test function we considered is the Branin function, defined as:

$$F(x_1, x_2) = [1 - 2x_2 + (1/20) \sin(4\pi x_2) - x_1]^2 + [x_2 - (1/2) \sin(2\pi x_1)]^2,$$

where $x_1, x_2 \in [-10, 10]$. This function has five global minimum points and the global minimum is 0. If we normalize the range of variables x_1 and x_2 into $[0, 1]$, then the five global minimal points are (0.55, 0.5), (0.50743, 0.52010), (0.52013, 0.51437), (0.57987, 0.48563) and (0.59257, 0.47990). The contour lines and the surface shape of the Branin function are shown in [Figs. 52](#) and [53](#), respectively. The five round dots in [Fig. 52](#) represent the global minimum points.

[Figures 54 ~ 57](#) show the optimization results after 500 function evaluations using DIRECT, DIRECT +, DIRECT-III and DIRECT-III +, respectively. The tiny dots in the figures on the left represent the sample points. The figures on the right are the local zoom-ins of the ones on the left, around the global minimum points. The centers of the circles denote the locations of the global minimum points.

[Figures 54](#) and [55](#) show that DIRECT and DIRECT + found all of the five global minimum points at this stage. [Figure 56](#) shows that only four global minimum points were found by the strongly locally biased DIRECT-III. Since the new locally biased partition strategy is applied to DIRECT-III, DIRECT-III + becomes even more locally biased than DIRECT-III and it only found three global minimum points, which is shown in [Fig. 57](#).

3.2.2 Tough test function case

The test function we considered here is an extremely “nasty” function called Shubert function. This function not only has 9 global minima, but it also has a total number of 400 local minimum points! The Shubert function is defined as follows:

$$F(x_1, x_2) = -\left(\sum_{i=1}^5 i \sin((i+1)x_1 + i) + \sum_{j=1}^5 j \sin((j+1)x_2 + j)\right) ,$$

where $x_1, x_2 \in [-10, 10]$. If we normalize the range of variables x_1 and x_2 into $[0, 1]$, then its 9 global minimum points are:

$$(0.1612712, 0.1612712),$$

$$(0.1612712, 0.4754305),$$

$$(0.1612712, 0.7895897),$$

$$(0.4754305, 0.1612712),$$

$$(0.4754305, 0.4754305),$$

$$(0.4754305, 0.7895897),$$

$$(0.7895897, 0.1612712),$$

$$(0.7895897, 0.4754305),$$

$$(0.7895897, 0.7895897).$$

The global minimum is -24.062499. The 3-D surface and 2-D contour of the Shubert function are shown in [Figs. 58](#) and [59](#), respectively. The nine solid dots in [Fig. 58](#) denote the nine global minimum points.

[Figures 60 ~ 63](#) show the optimization results after 2500 function evaluations using DIRECT, DIRECT +, DIRECT-III and DIRECT-III +, respectively. The tiny dots in these

represent the sample points generated and the centers of the circles denote the locations of the global minimum points.

Figures 60, 61 and 62 show that DIRECT, DIRECT+ and DIRECT-III found all of the nine global minimum points at this stage, while Fig. 63 shows that only eight global minimum points were found by the most locally biased DIRECT-III +.

In order to find all nine global minima by using DIRECT-III +, we present two ways here. The first method is quite straightforward: increasing the number of function evaluations. Figure 64 shows the results after 4500 function evaluations by using DIRECT-III +. We see that all nine global minimum points were found. The second method is to introduce some globally biased factors for the DIRECT-III + to compensate some of its strongly locally biased properties. Here we define 0.01 tolerance for both x_1 and x_2 variables. Figure 65 shows the results after 2500 function evaluations by using DIRECT-III +. It is clear that by defining the tolerance, DIRECT-III + found all the global minima within the same number of function evaluations.

3.3 Summary of the numerical experiments

We performed extensive numerical experiments by using test functions with single global minimum and multiple global minima.

For test functions with single global minimum point, all the four algorithms, namely DIRECT, DIRECT +, DIRECT-III and DIRECT-III + found the global minimum point for each case. In all the cases, the new partition strategy results in a higher convergence rate than does the standard partition strategy with respect to either DIRECT or DIRECT-III. Especially, when the new strategy is applied to DIRECT-III, the resulting DIRECT-III + has the highest convergence rate among the four algorithms.

For test functions with multiple global minimum points, DIRECT-III + fails to find all the global minimum points for tough test function compared with the other three algorithms. This is due to its highly locally biased property. The remedy for that is either to increase the number of function evaluations, or, more effectively, to adopt some globally biased features such as defining the tolerance.

Next we will discuss the performance of DIRECT, DIRECT+, DIRECT-III and DIRECT-III + in the slider Air Bearing Surface (ABS) optimization.

4. SLIDER AIR BEARING DESIGN OPTIMIZATION CASE

4.1 Air bearing design optimization problem

The optimization problem defined here is: given a prototype slider ABS design, optimize it to get uniform flying heights near the target flying height and a flat roll profile across the disk. Also increase its air bearing stiffness if possible.

Here the NSIC 7nm flying height slider is used as the prototype slider. The rail shape and the 3-dimensional rail geometry are shown in [Figs. 66](#) and [67](#), respectively.

The slider is a Pico slider (1.25×1.0mm), which flies over a disk rotating at 7200 RPM. Its flying heights are all around 7nm from OD to ID. Now we want to lower its flying heights to the target flying height, i.e. 5nm and at the same time maintain a flat roll profile at the three different radial positions OD, MD and ID. The objective function or cost function is defined as:

$$\begin{aligned}
 & 1 \times (FH \text{ Max Difference term}) + 9 \times (FH \text{ term}) + 1 \times (Roll \text{ term}) + \\
 & 1 \times (Roll \text{ Cutoff term}) + 1 \times (Pitch \text{ Cutoff term}) + 1 \times (Vertical \text{ Sensitivity term}) + \\
 & 1 \times (Pitch \text{ Sensitivity term}) + 1 \times (Roll \text{ Sensitivity term}) + 1 \times (Negative \text{ Force term}) .
 \end{aligned}$$

So the goal of the optimization is to minimize this multi-objective function under the given constraints. Note that since we are primarily concerned with the flying heights, we put a heavier weight (9) on that term. All the objective terms are normalized and their definitions can be found in CML technical report [01-016](#).

[Figure 68](#) shows that 2 original constraint points are defined for this case. These 2 constraint points can move along the length direction within the intervals prescribed. To maintain a symmetric ABS design and the fixed local rail shape we also defined the symmetric constraints and the relative constraints.

4.2 Optimization results

Using the initial design, constraints and objective function, we carried out the optimization using DIRECT, DIRECT +, DIRECT-III and DIRECT-III +, respectively. [Figures 69 ~ 72](#) show the variation of the objective function value by using DIRECT, DIRECT +, DIRECT-III and DIRECT-III +, respectively. And [Fig. 73](#) shows the convergence comparison. For this testing case, all four algorithms show a similarly fast convergence rate. The best objective function values obtained by using DIRECT, DIRECT +, DIRECT-III and DIRECT-III + are 5.571, 5.571, 5.56 and 5.553. Since the smaller the objective function value the better the design, DIRECT-III + found slightly better ABS design than did DIRECT, DIRECT + and DIRECT-III.

[Figures 74 ~ 77](#) show the optimization results after 200 function evaluations using DIRECT, DIRECT +, DIRECT-III and DIRECT-III +, respectively. The tiny dots in these represent the sample ABS designs generated and the circles denote the locations of the optimized ABS designs. Again, the new partition strategy shows locally biased property by leaving larger unexplored area in [Figs. 75 and 77](#).

[Figures 78 ~ 81](#) show the final optimized ABS designs obtained by using DIRECT, DIRECT-I, DIRECT-II and DIRECT-III, respectively. In these figures, the gray lines show the rail shape of the initial design and the dark lines show the rail shape of the optimized design. The four optimized ABS designs are very similar to each other. All four optimized

ABS designs have very uniform flying heights around the target 5nm FH, and a reasonably flat roll profile, which are shown in [Figs. 82](#) and [83](#).

5. *CONCLUSION*

We performed extensive numerical experiments using test functions with single global minimum and multiple global minima.

For test functions with single global minimum point, DIRECT, DIRECT +, DIRECT-III and DIRECT-III + all found the global minimum point for each case. In all the cases, the new partition strategy results in a higher convergence rate than does the standard partition strategy with respect to either DIRECT or DIRECT-III. And DIRECT-III + has the highest convergence rate among the four algorithms in the long run.

For test functions with multiple global minimum points, though DIRECT-III + has the highest convergence rate, it fails to find all the global minimum points for tough test function compared with the other three algorithms. This is due to its highly locally biased property. The remedy for that is either to increase the number of function evaluations, or, more effectively, to adopt some globally biased features such as defining the tolerance.

The slider ABS optimization problem is a strongly nonlinear problem. The results of the test case show very similar performance for DIRECT, DIRECT +, DIRECT-III and

DIRECT-III +. In the 2-D testing case, DIRECT-III + found slightly better ABS design than did DIRECT, DIRECT + and DIRECT-III.

In summary, the new partition strategy can increase the convergence rate for the DIRECT algorithm and its variations. DIRECT-III + has the highest convergence rate compared with DIRECT, DIRECT + and DIRECT-III and it shows amazingly high convergence rate for some high dimensional monotonic test function cases. It is expected to perform better for higher dimension ABS optimization problems.

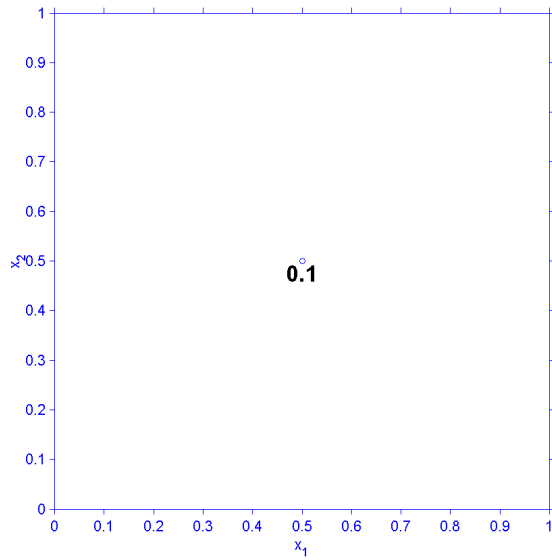
ACKNOWLEDGEMENT

This study is supported by the Computer Mechanics Laboratory (CML) at the University of California at Berkeley and partially supported by the Extremely High Density Recordings (EHDR) project of the Information Storage Industry Consortium (INSIC).

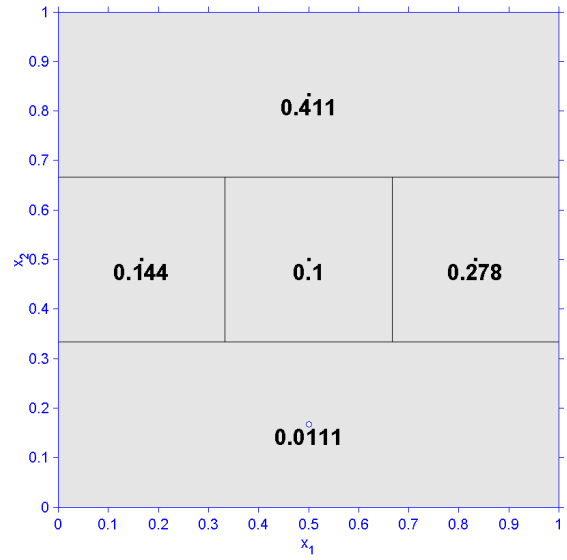
REFERENCES

1. Zhu, H. and Bogy, D., 2001, "DIRECT Algorithm and its Application to Slider Air Bearing Surfaces Optimization", Technical Report 01-003, Computer Mechanics Laboratory, University of California at Berkeley.
2. Zhu, H. and Bogy, D., 2001, "Locally Biased Variations of the DIRECT Algorithm and their application to the Slider Air Bearing Surfaces Optimization", Technical Report 01-007, Computer Mechanics Laboratory, University of California at Berkeley.
3. Zhu, H. and Bogy, D., 2001, "Modifications to the DIRECT Algorithm", Technical Report 01-013, Computer Mechanics Laboratory, University of California at Berkeley.
4. Zhu, H. and Bogy, D., 2001, "The CML Air Bearing Optimization Program Version 2.0", Technical Report 01-016, Computer Mechanics Laboratory, University of California at Berkeley.
5. Zhu, H. and Bogy, D., 2002, "DIRECT Algorithm and Its Application To Slider Air Bearing Surface Optimization", *Intermag 2002 Conference*, Amsterdam, The Netherlands.

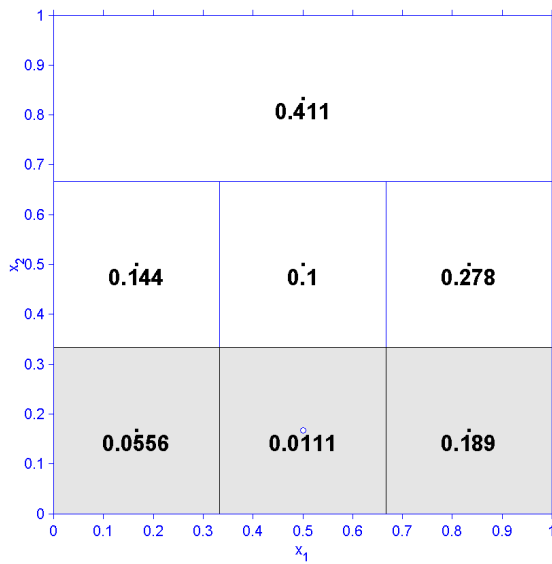
6. Zhu, H. and Bogy, D., 2002, "Hard disk drive air bearing design: Modified DIRECT algorithm and its application to slider Air Bearing Surface optimization", 6th *International Tribology Conference (AUSTRIB '02)*, Western Australia.
7. Bogy, D., Wu, L., Zeng, Q-H and Zhu, H., 1999, "Air Bearing Designs for 100 Gbit/in²", TRIB-Vol. 9, *Proceedings of the Symposium on Interface Technology Towards 100 Gbit/in²*, ASME, pp. 11-16
8. Bogy, D., Fong, W., Thornton, B., Zhu, H., Gross, H. and Bhatia, C., 2002, "Some Tribology and Mechanics Issues for 100 Gbit/in² HDD", *Intermag 2002 Conference*, Amsterdam, The Netherlands.
9. Jones, D. R., Perttunen, C. D. and Stuckman, B. E., 1993, "Lipschitzian Optimization Without the Lipschitz Constant ", *Journal of Optimization Theory and Application*, Vol. 79, No. 1, pp. 157-181.
10. Gablonsky, J. M., 1998, "An Implementation of the DIRECT algorithm", Technical Report CRSC-TR98-29, Center for Research in Scientific Computation, North Carolina State University.
11. Gablonsky, J. M. and Kelley, C. T., 2000, "A locally-biased form of the DIRECT algorithm", Technical Report CRSC-TR00-31, Center for Research in Scientific Computation, North Carolina State University.



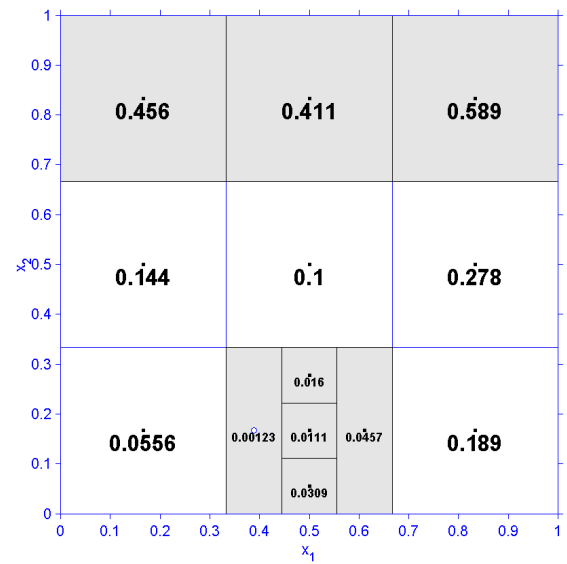
A. Initial state



B. Iteration 1

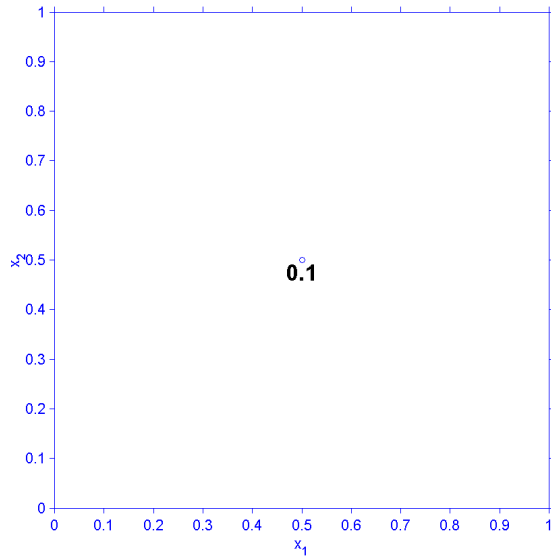


C. Iteration 2

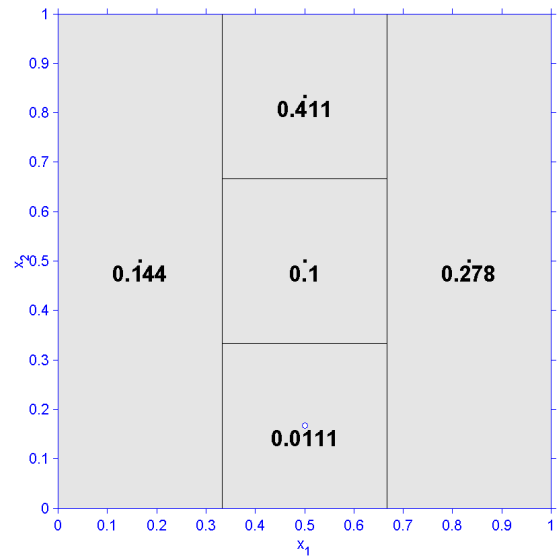


D. Iteration 3

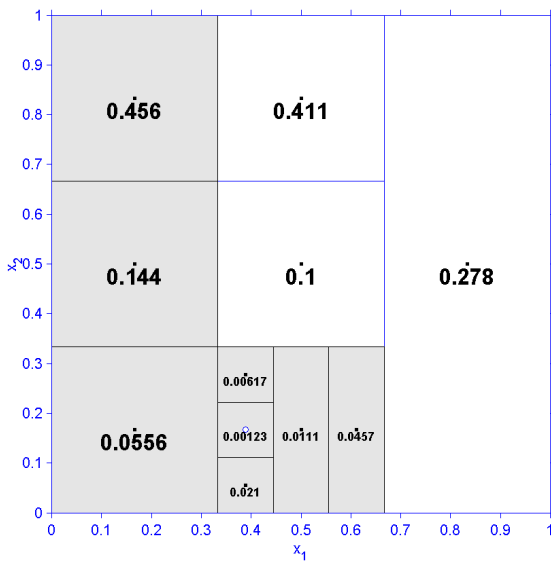
Fig. 1 Demonstration of the standard partition strategy



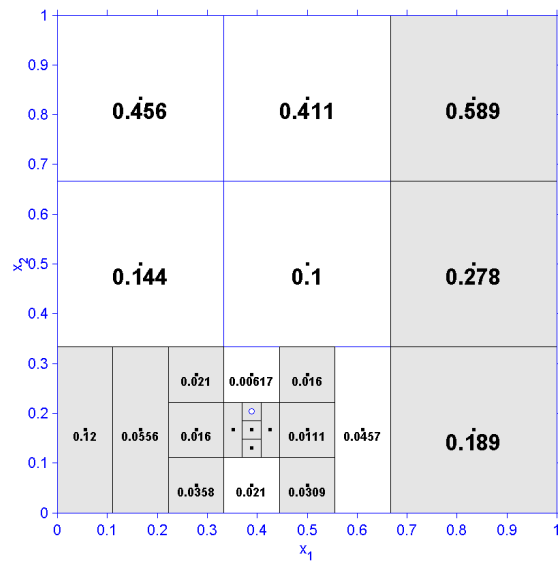
A. Initial state



B. Iteration 1



C. Iteration 2



D. Iteration 3

Fig. 2 Demonstration of the new partition strategy

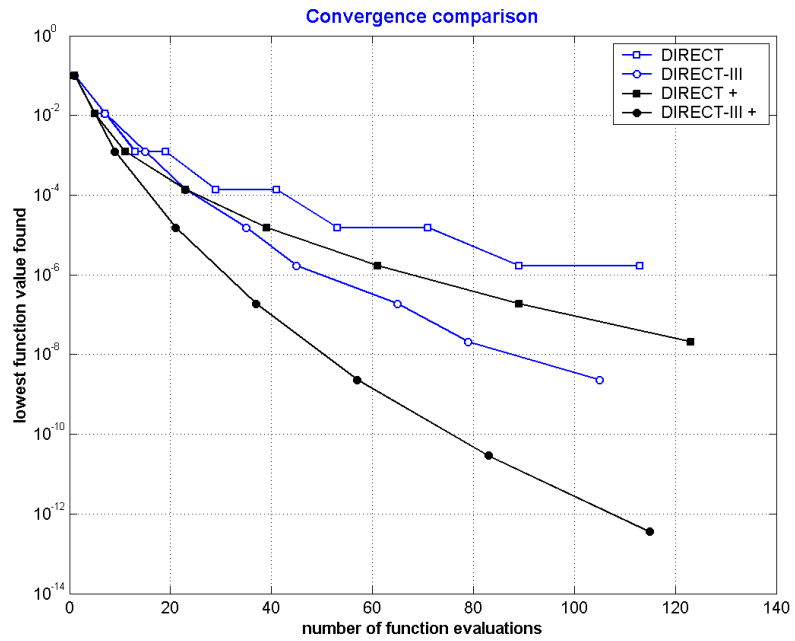


Fig. 3 Convergence comparison for 2-D case

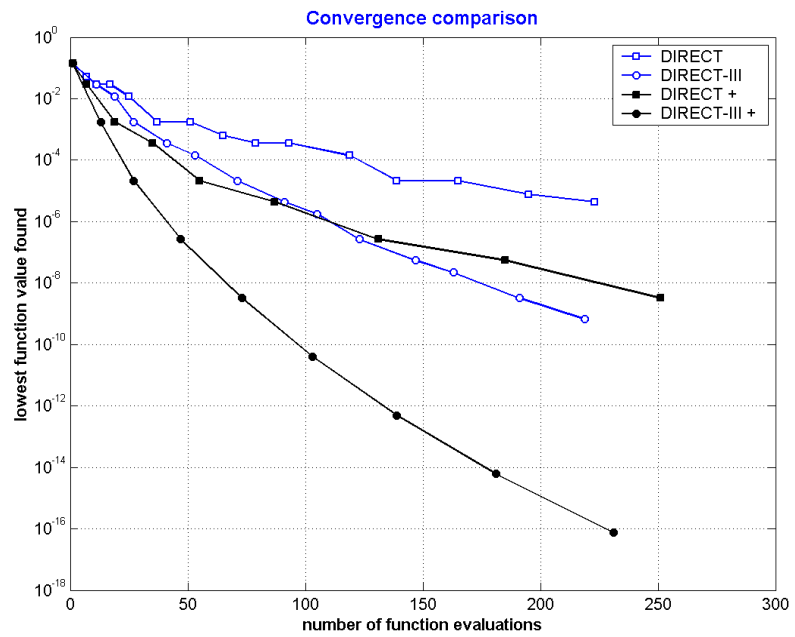


Fig. 4 Convergence comparison for 3-D case

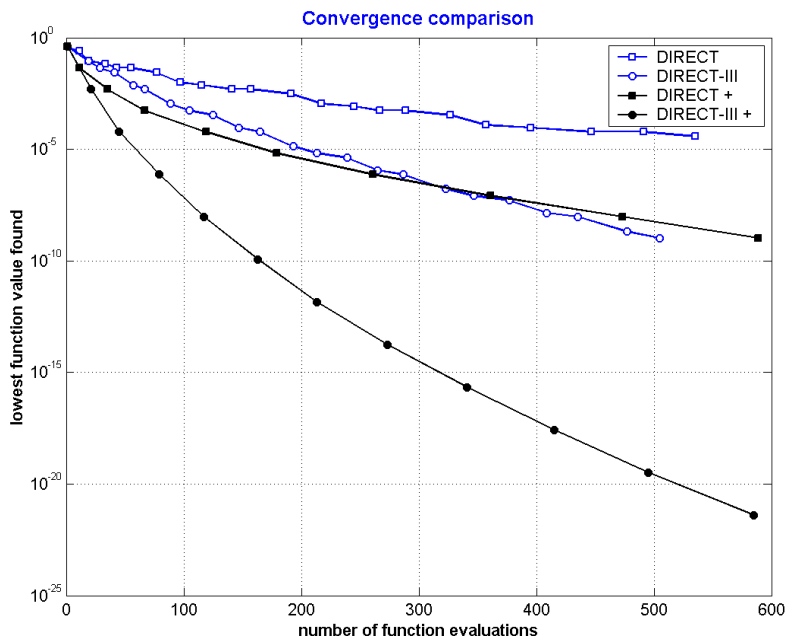


Fig. 5 Convergence comparison for 5-D case

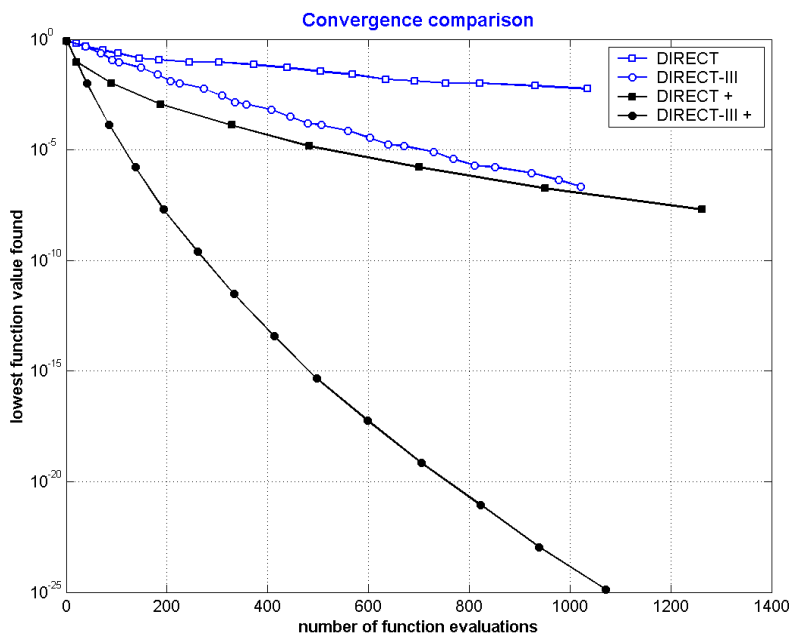


Fig. 6 Convergence comparison for 10-D case

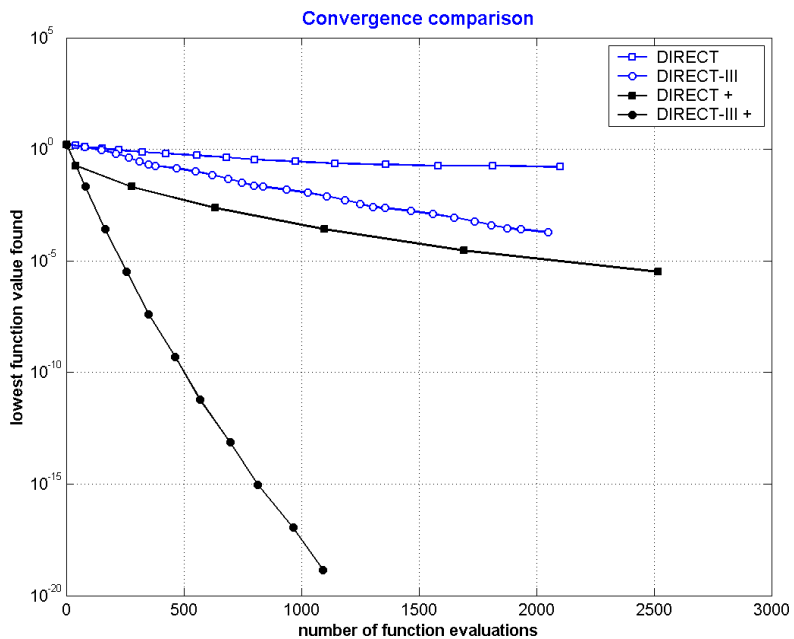


Fig. 7 Convergence comparison for 20-D case

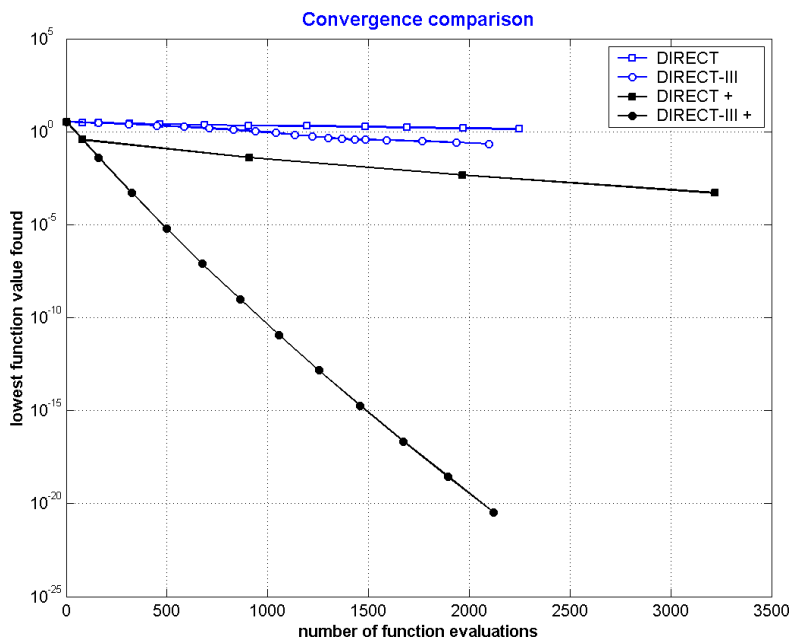


Fig. 8 Convergence comparison for 40-D case

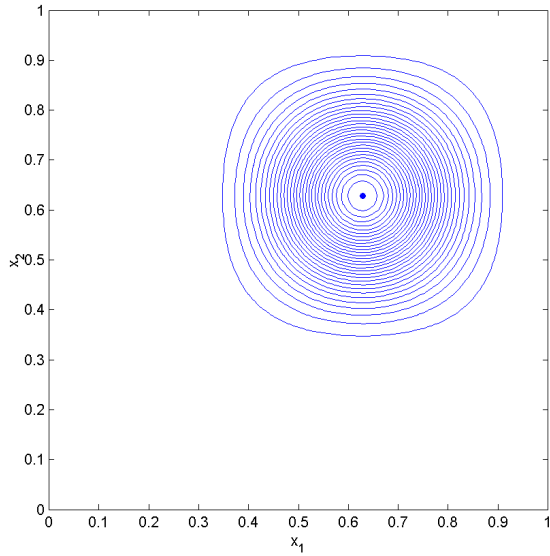


Fig. 9 Contour lines of Easom function

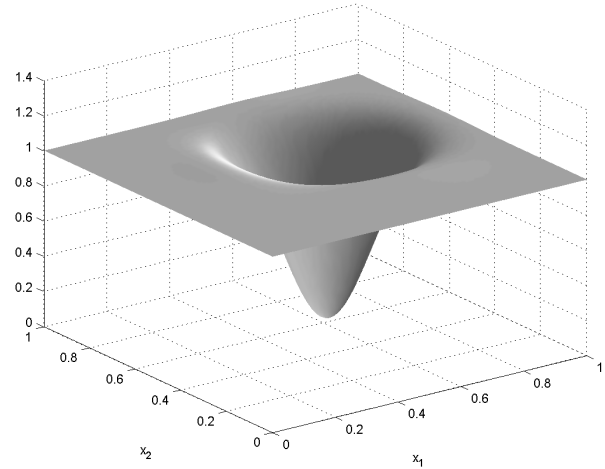


Fig. 10 Surface shape of Easom function

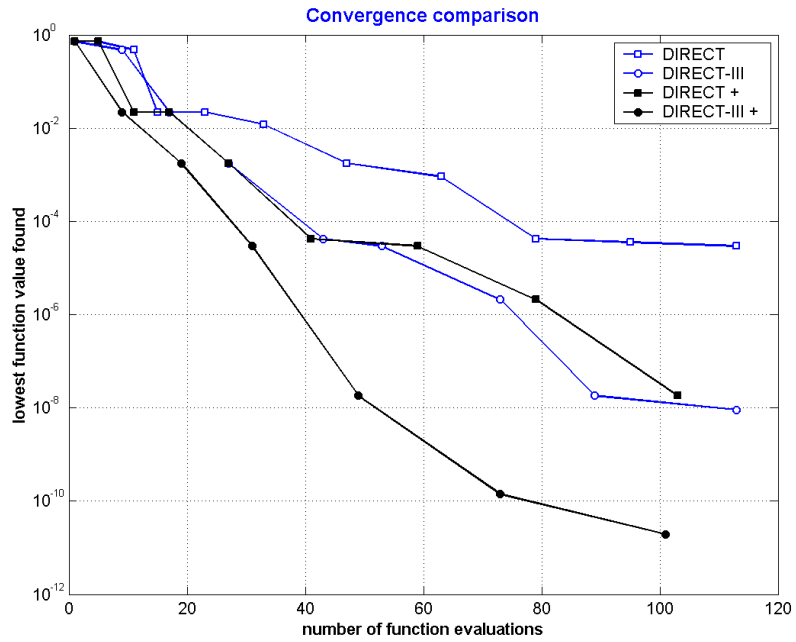


Fig. 11 Convergence comparison for Easom function case

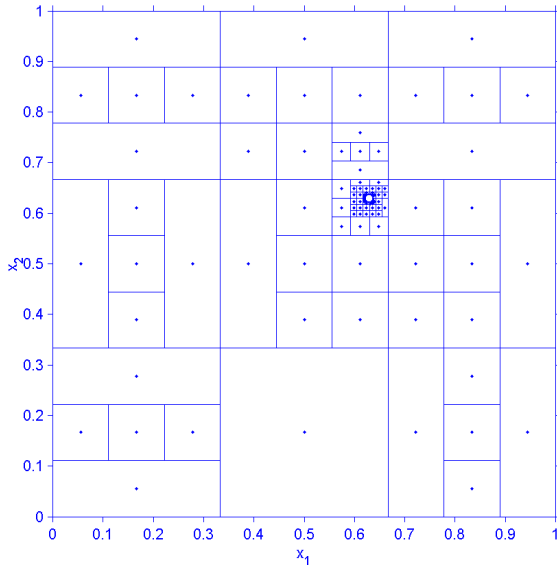


Fig. 12 Results of DIRECT

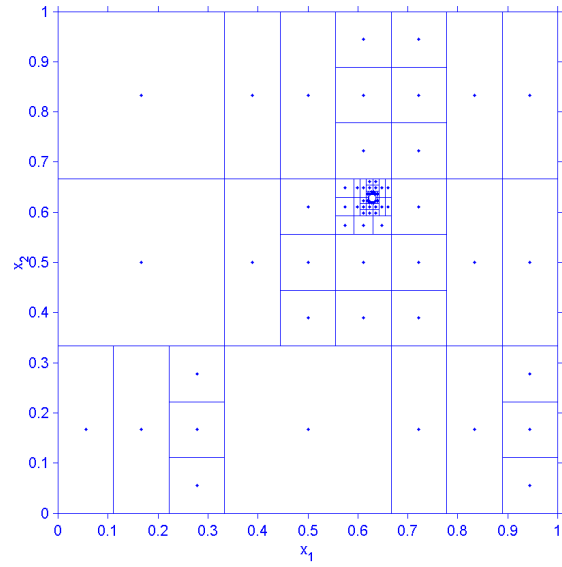


Fig. 13 Results of DIRECT +

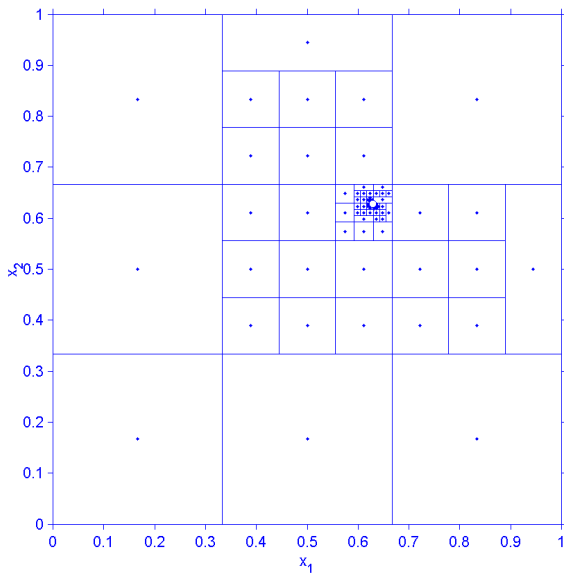


Fig. 14 Results of DIRECT-III

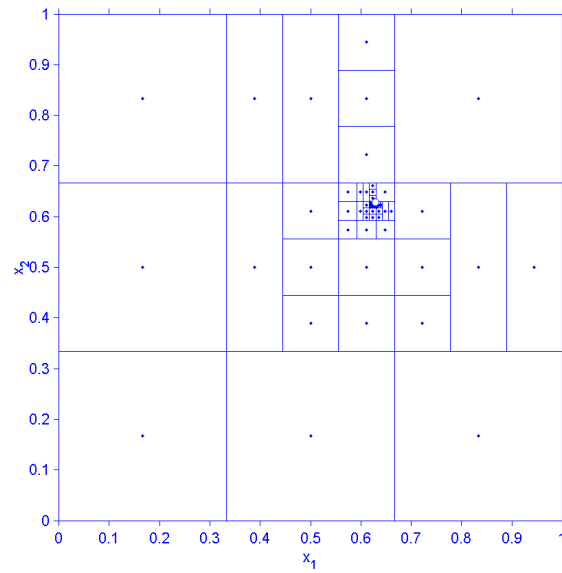


Fig. 15 Results of DIRECT-III +

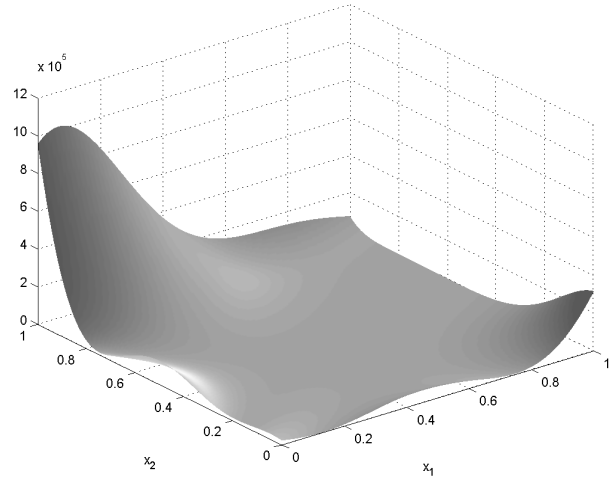
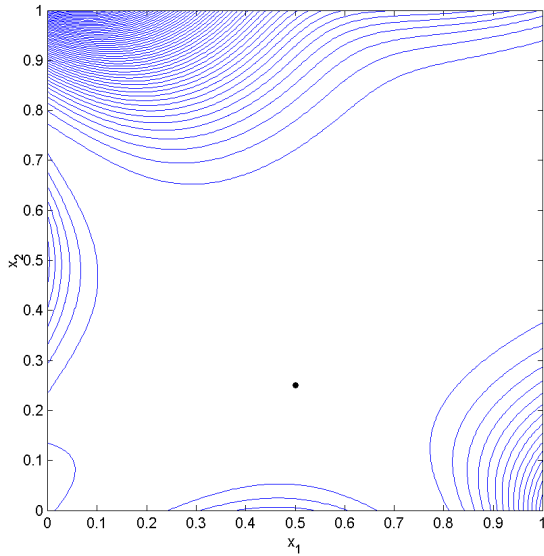


Fig. 16 Contour lines of Goldstein function

Fig. 17 Surface shape of Goldstein function

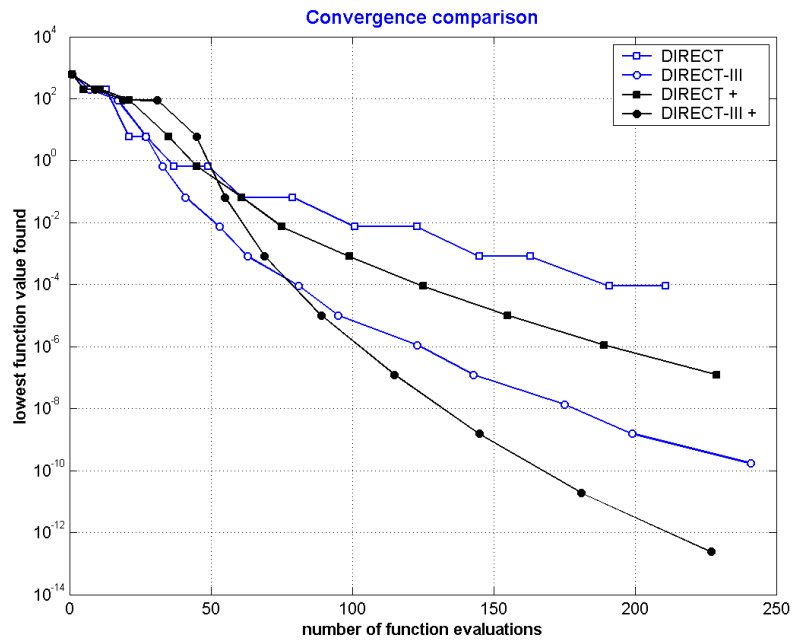


Fig. 18 Convergence comparison for Goldstein Price function case

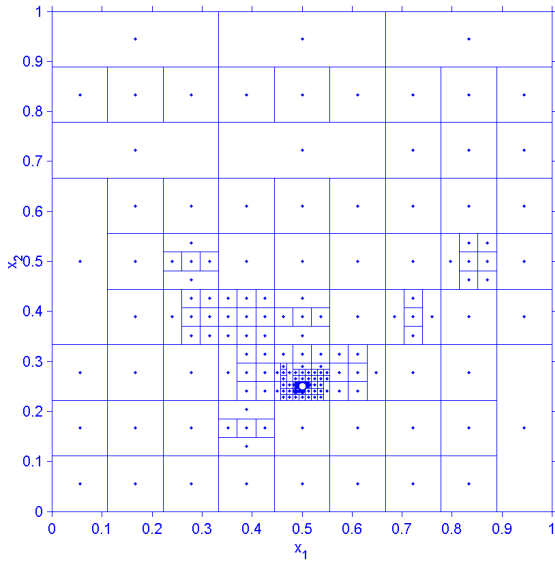


Fig. 19 Results of DIRECT

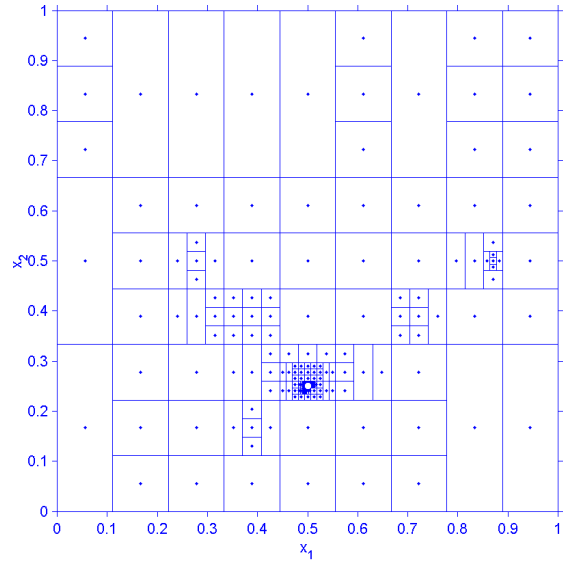


Fig. 20 Results of DIRECT +

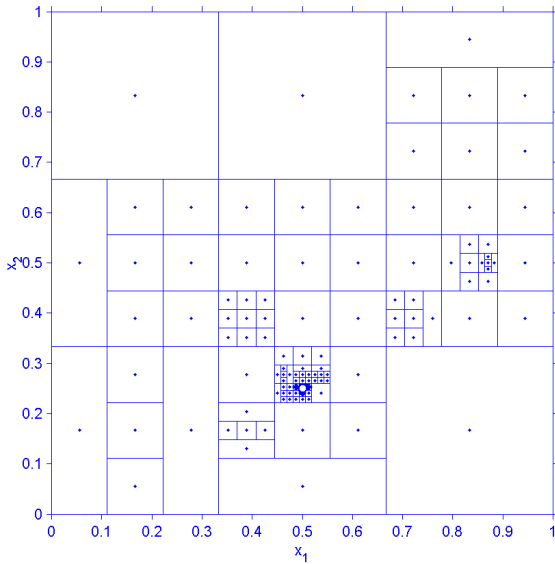


Fig. 21 Results of DIRECT-III

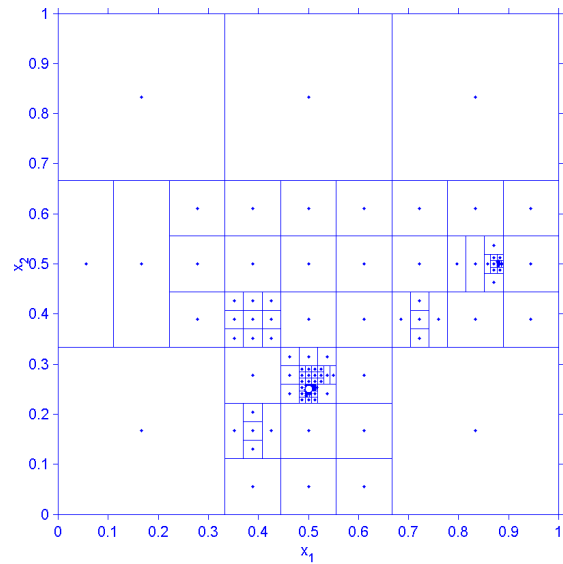


Fig. 22 Results of DIRECT-III +

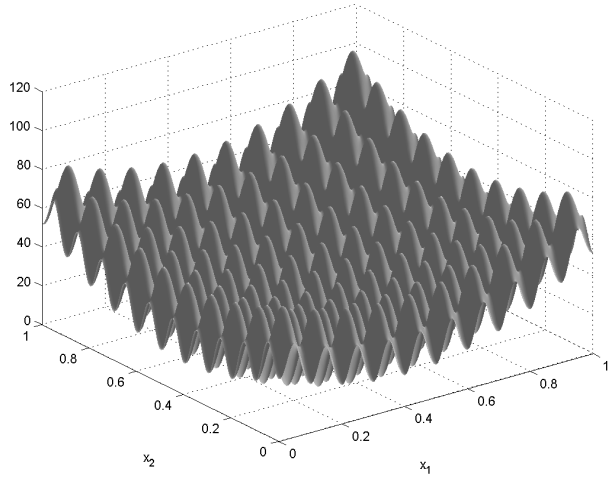
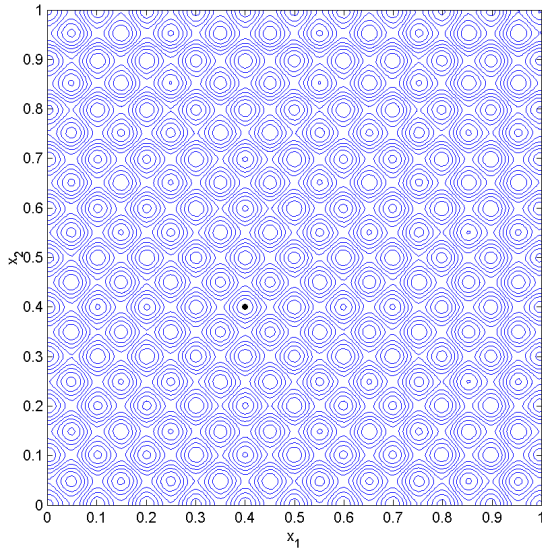


Fig. 23 Contour lines of Rastrigin function Fig. 24 Surface shape of Rastrigin function

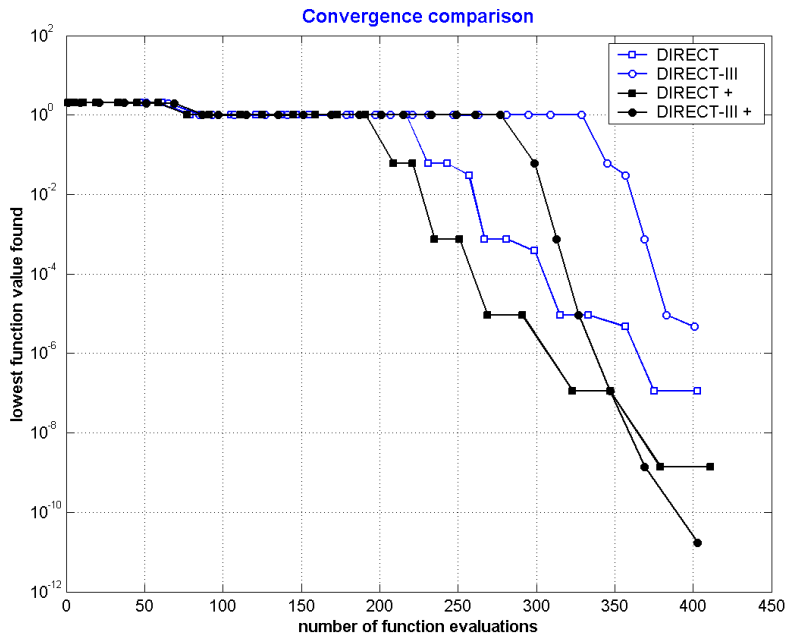


Fig. 25 Convergence comparison for Rastrigin function case

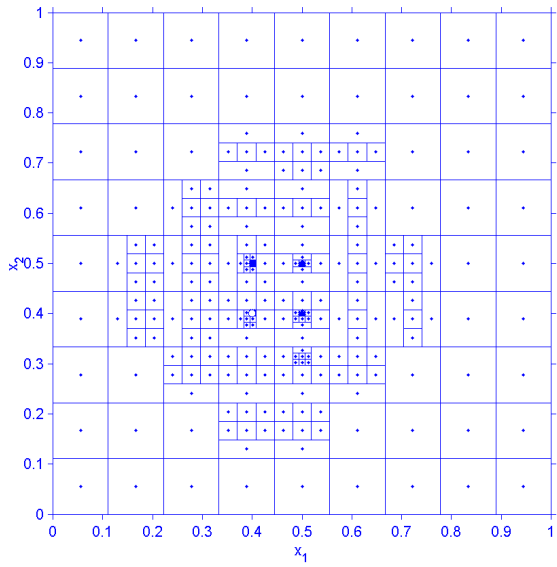


Fig. 26 Results of DIRECT

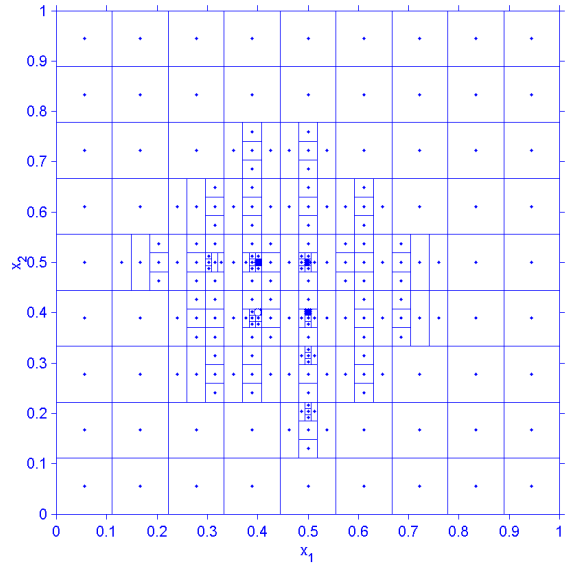


Fig. 27 Results of DIRECT +

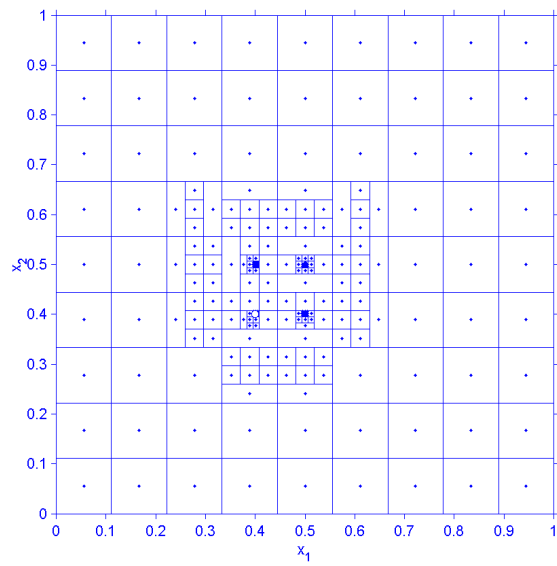


Fig. 28 Results of DIRECT-III

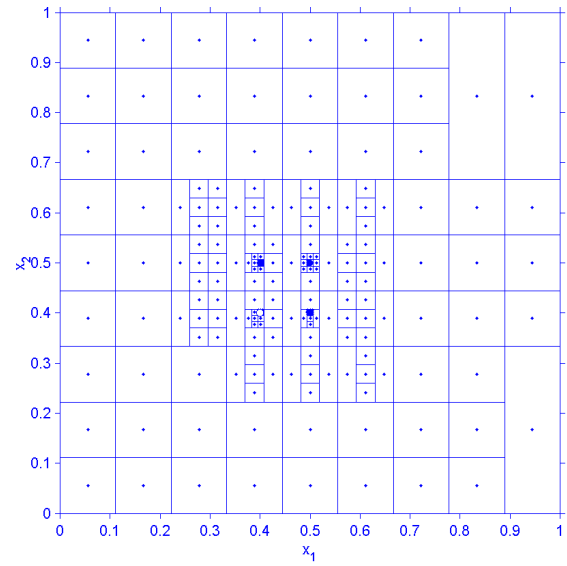


Fig. 29 Results of DIRECT-III +

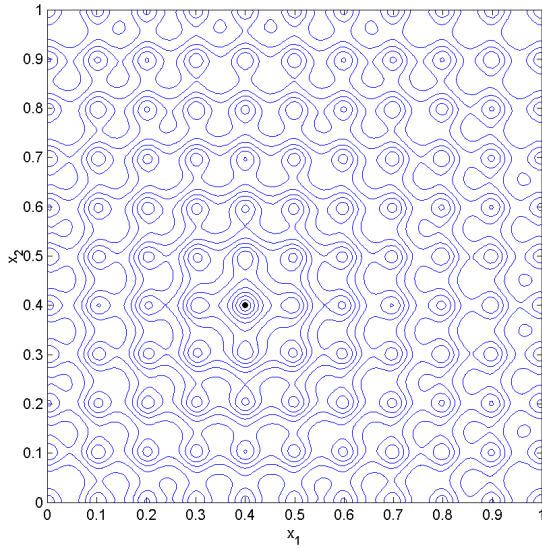


Fig. 30 Contour lines of Ackely function

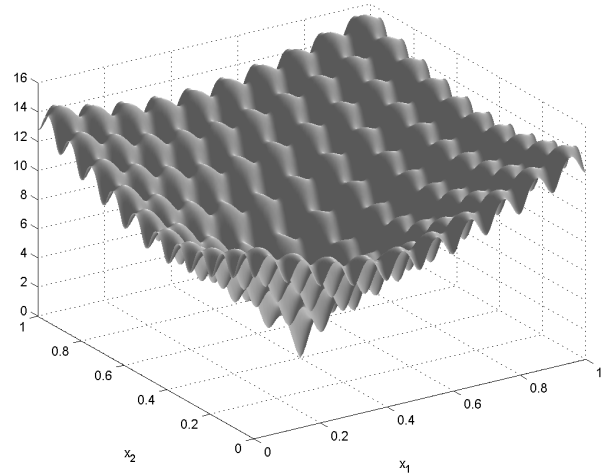


Fig. 31 Surface shape of Ackely function

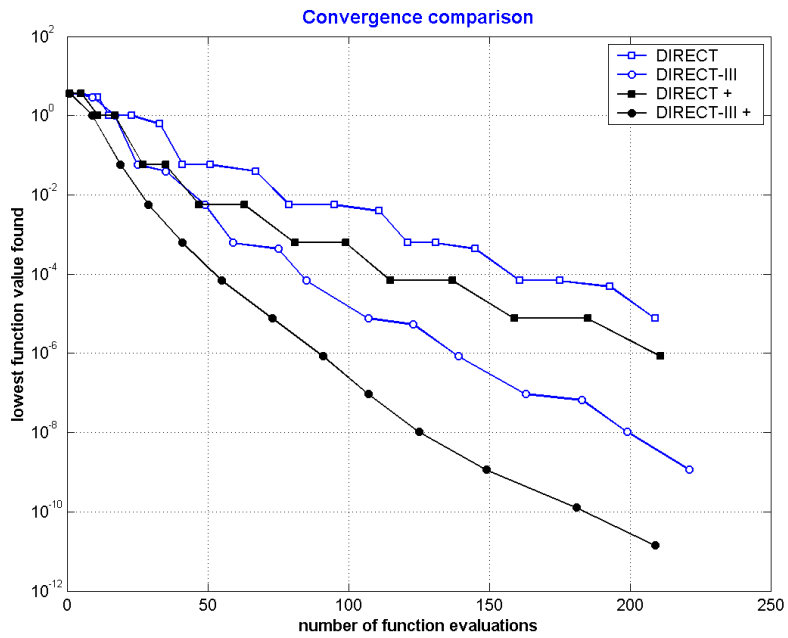


Fig. 32 Convergence comparison for Ackley's Path function case

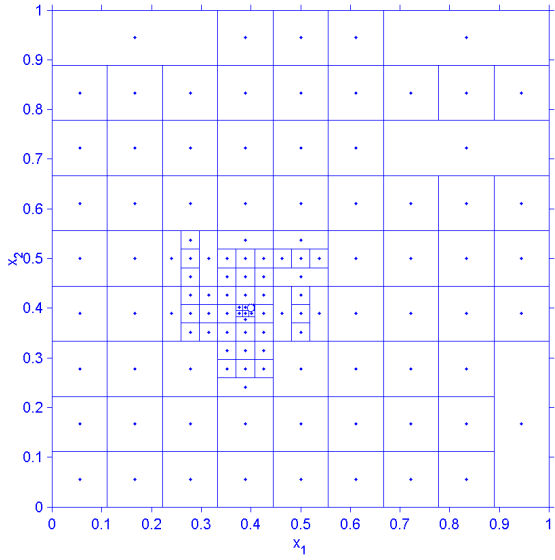


Fig. 33 Results of DIRECT

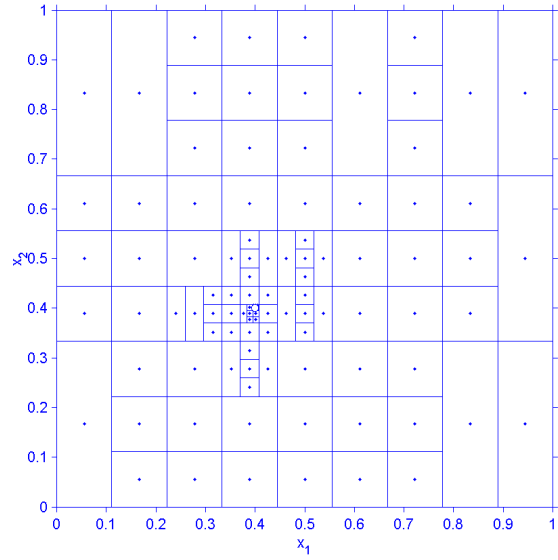


Fig. 34 Results of DIRECT +

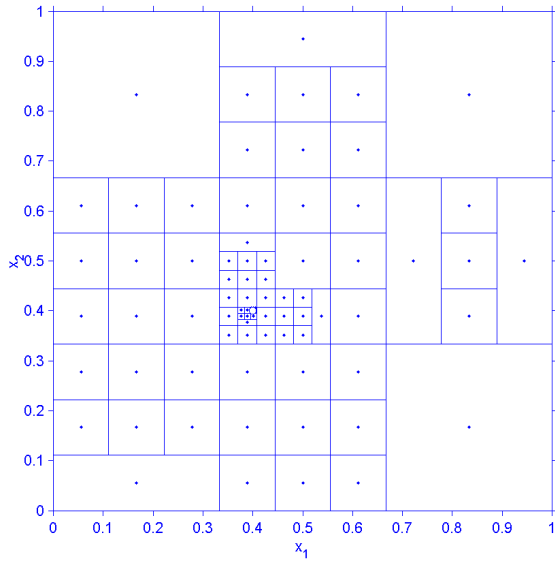


Fig. 35 Results of DIRECT-III

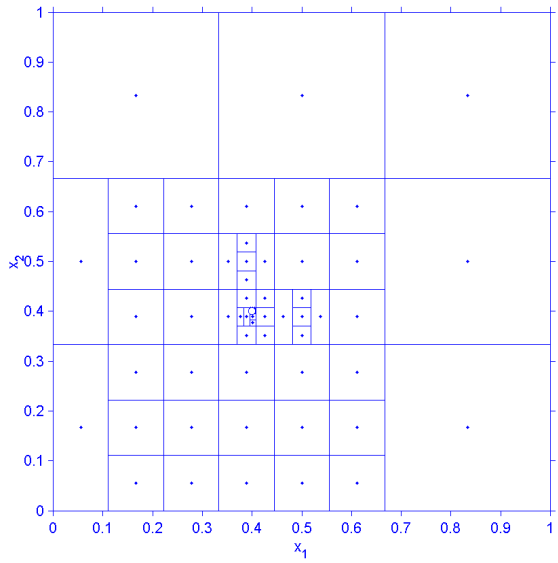


Fig. 36 Results of DIRECT-III +

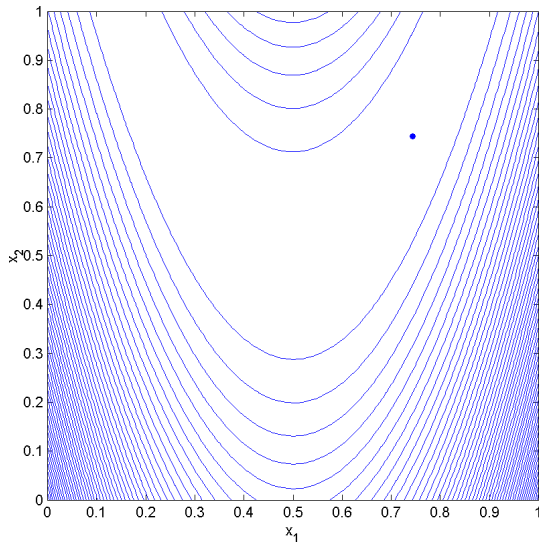


Fig. 37 Contour lines of R-B function

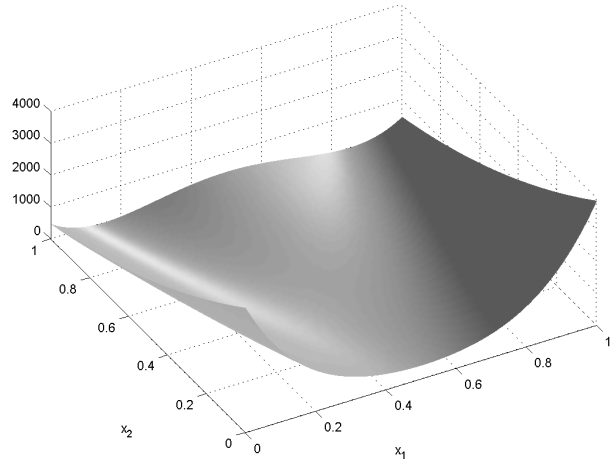


Fig. 38 Surface shape of R-B function

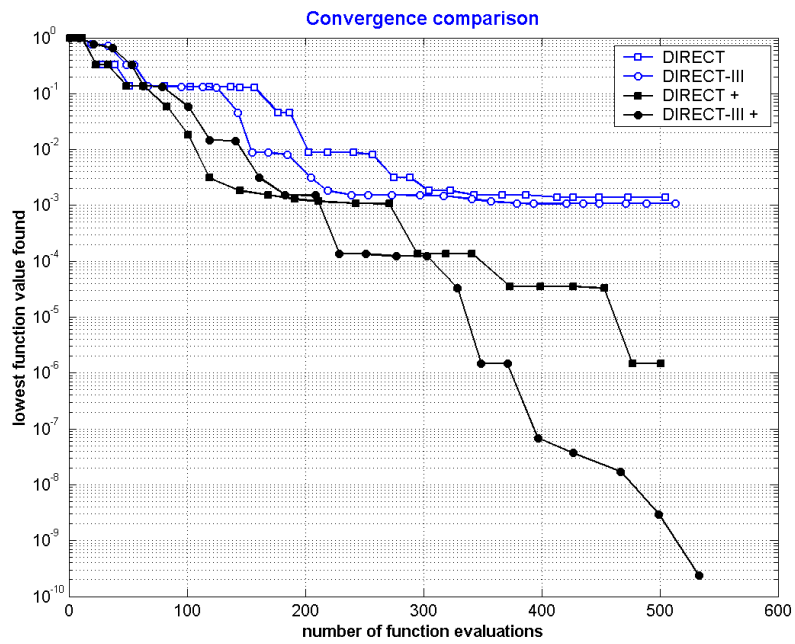


Fig. 39 Convergence comparison for Rosen Brock function case

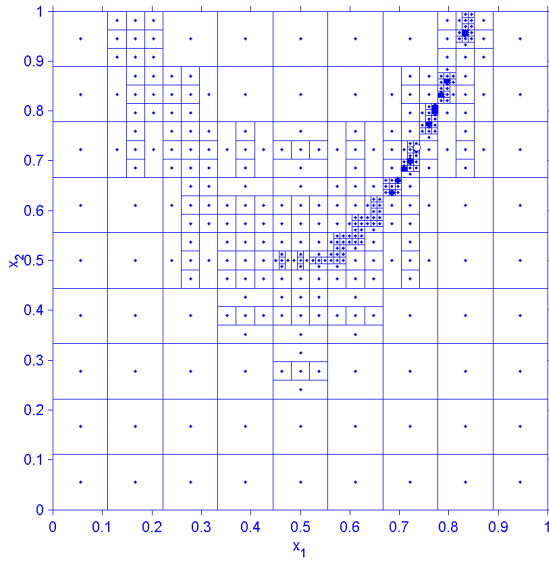


Fig. 40 Results of DIRECT

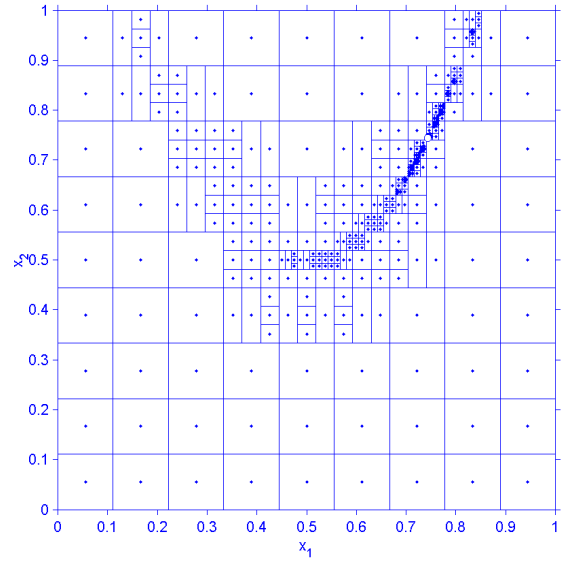


Fig. 41 Results of DIRECT +

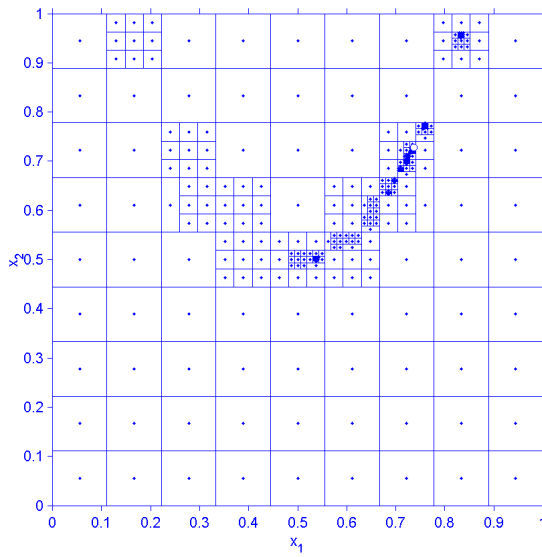


Fig. 42 Results of DIRECT-III

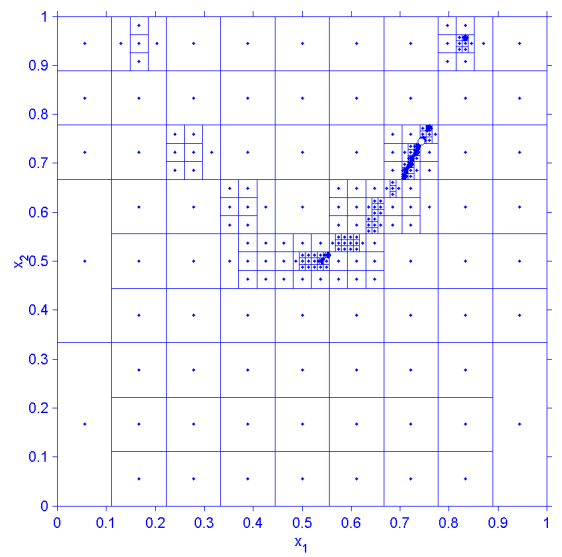


Fig. 43 Results of DIRECT-III +

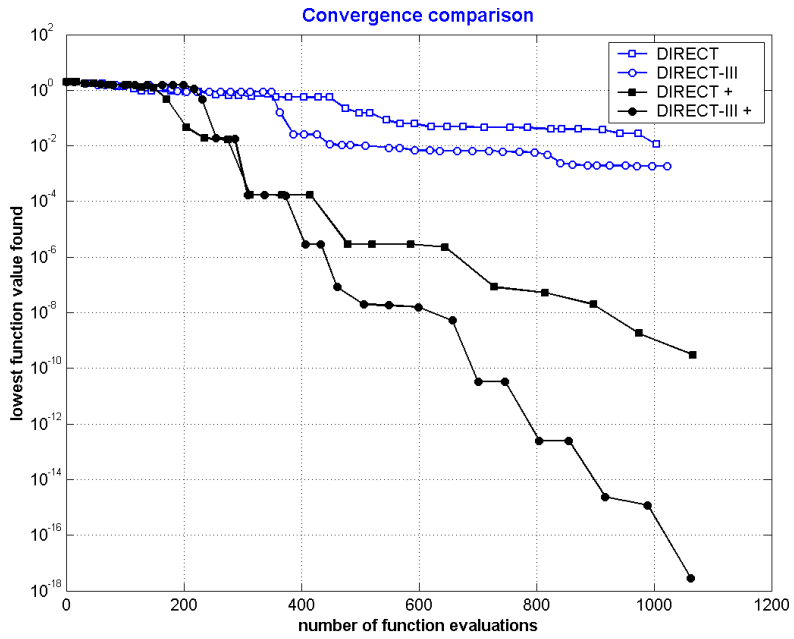


Fig. 44 Convergence comparison for 3-D Rosen Brock function case

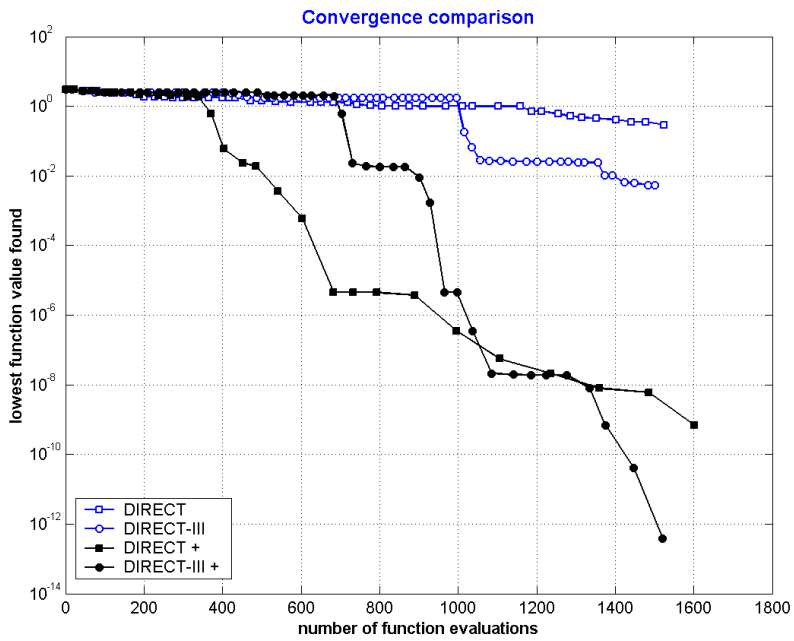


Fig. 45 Convergence comparison for 4-D Rosen Brock function case

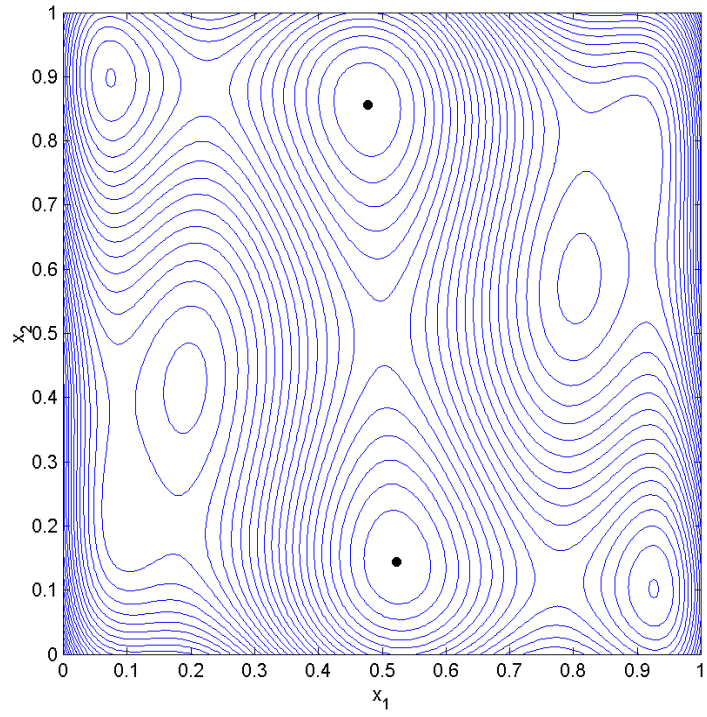


Fig. 46 Contour lines of Six-hump function

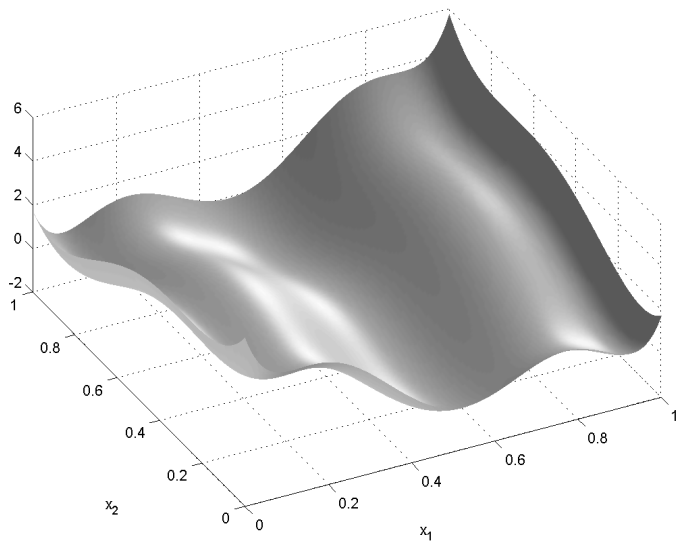


Fig. 47 Surface shape of Six-hump function

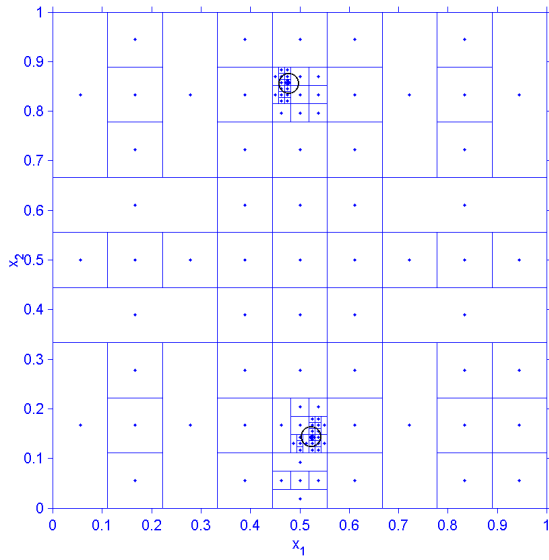


Fig. 48 Results of DIRECT

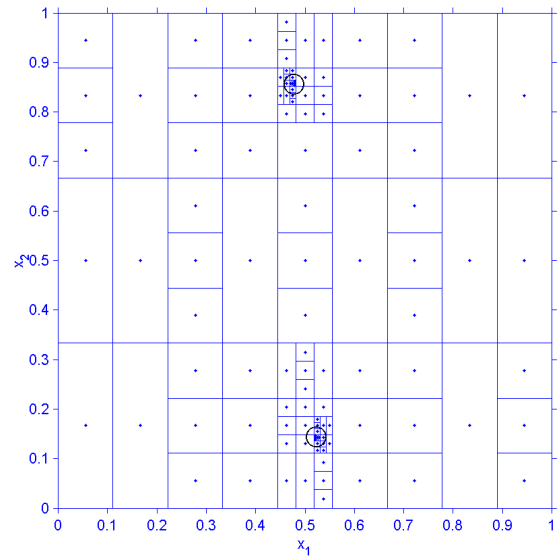


Fig. 49 Results of DIRECT +

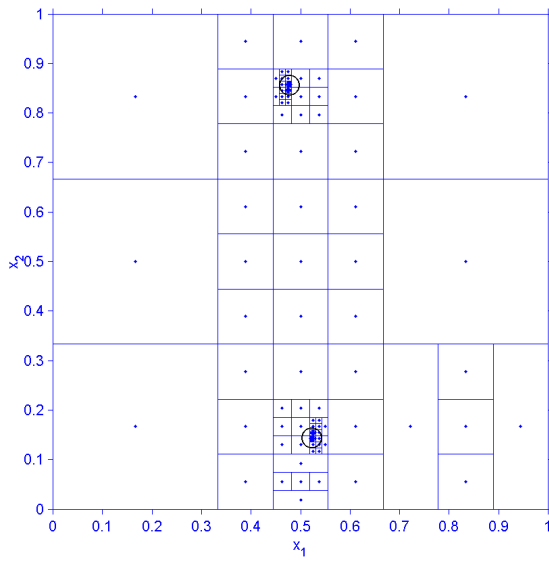


Fig. 50 Results of DIRECT-III

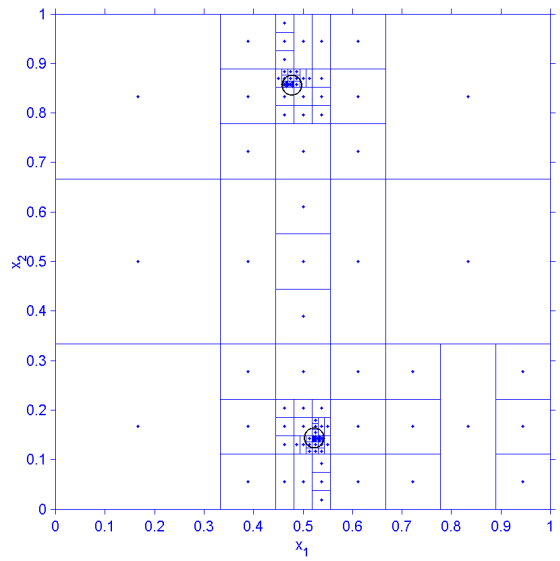


Fig. 51 Results of DIRECT-III +

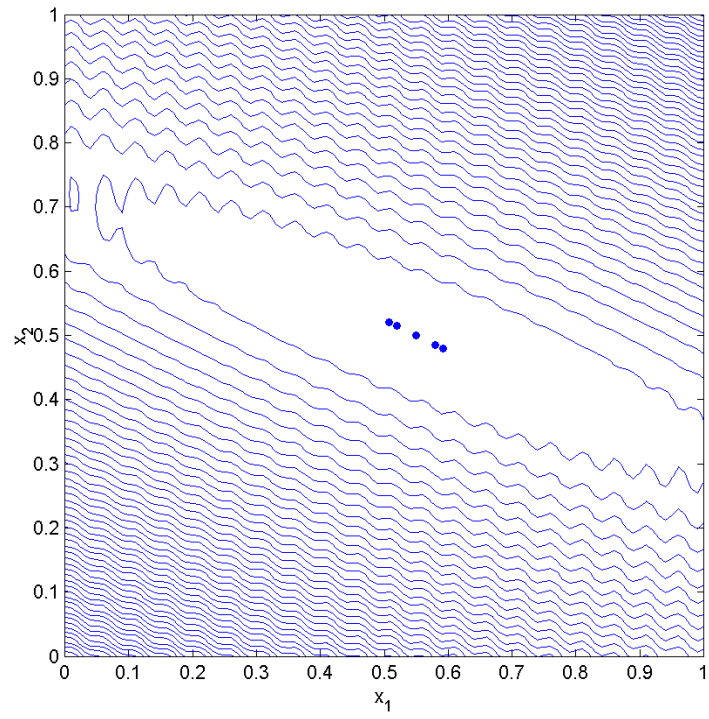


Fig. 52 Contour lines of Branin function

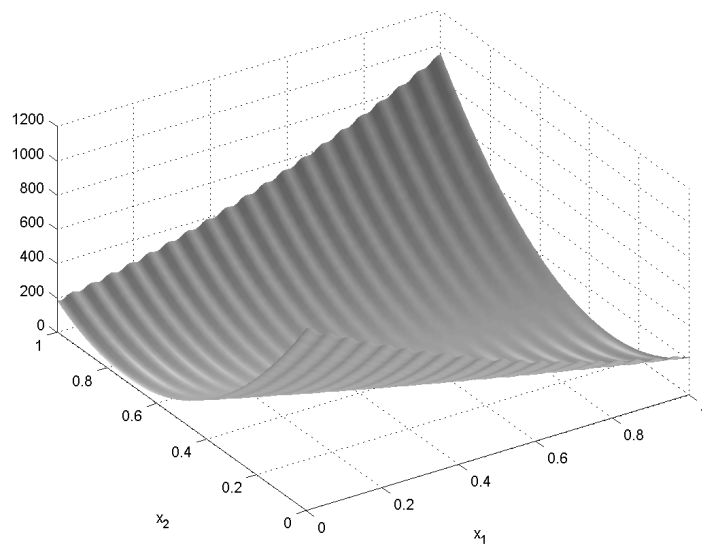


Fig. 53 Surface shape of Branin function

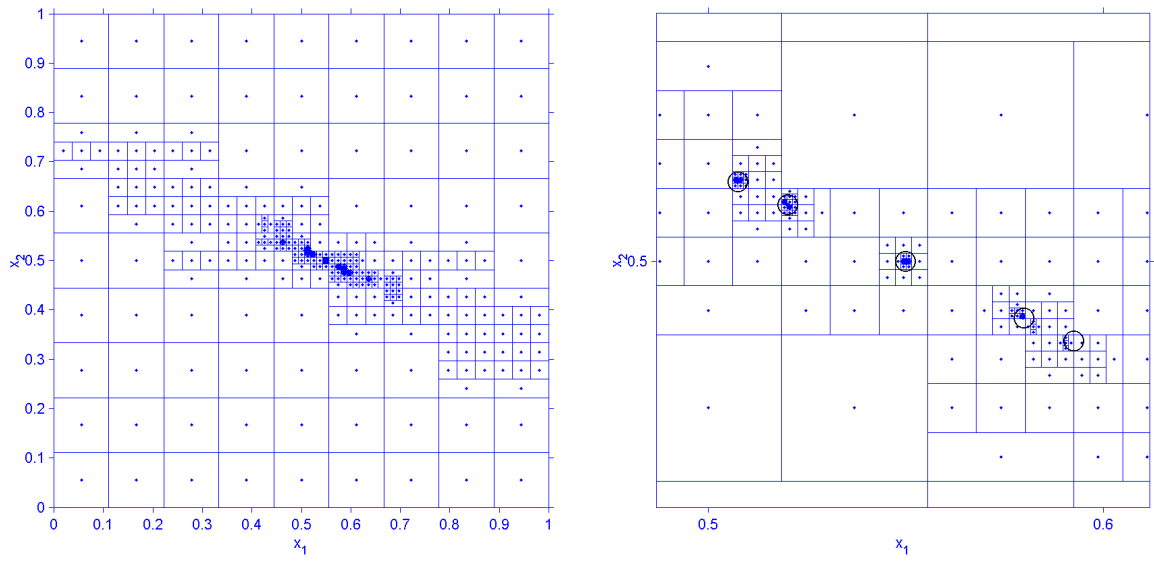


Fig. 54 Results of DIRECT and the local zoom-in

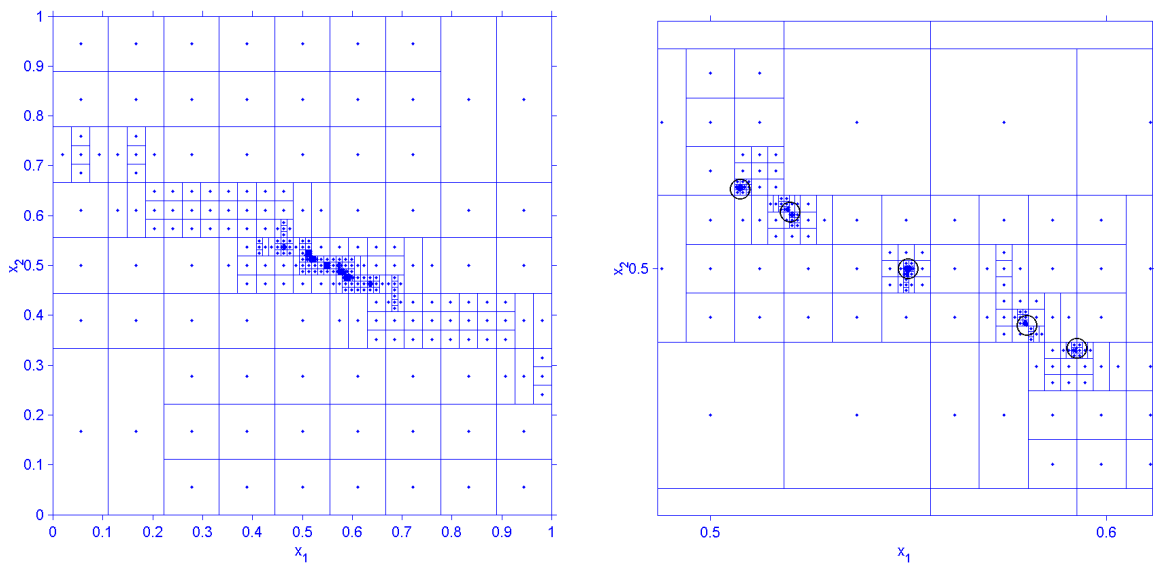


Fig. 55 Results of DIRECT+ and the local zoom-in

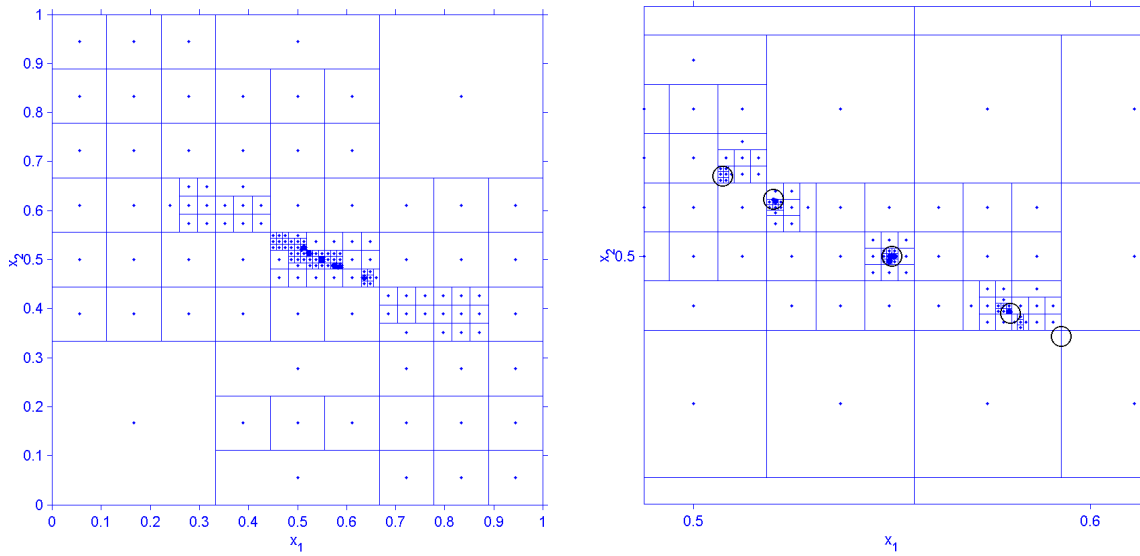


Fig. 56 Results of DIRECT-III and the local zoom-in

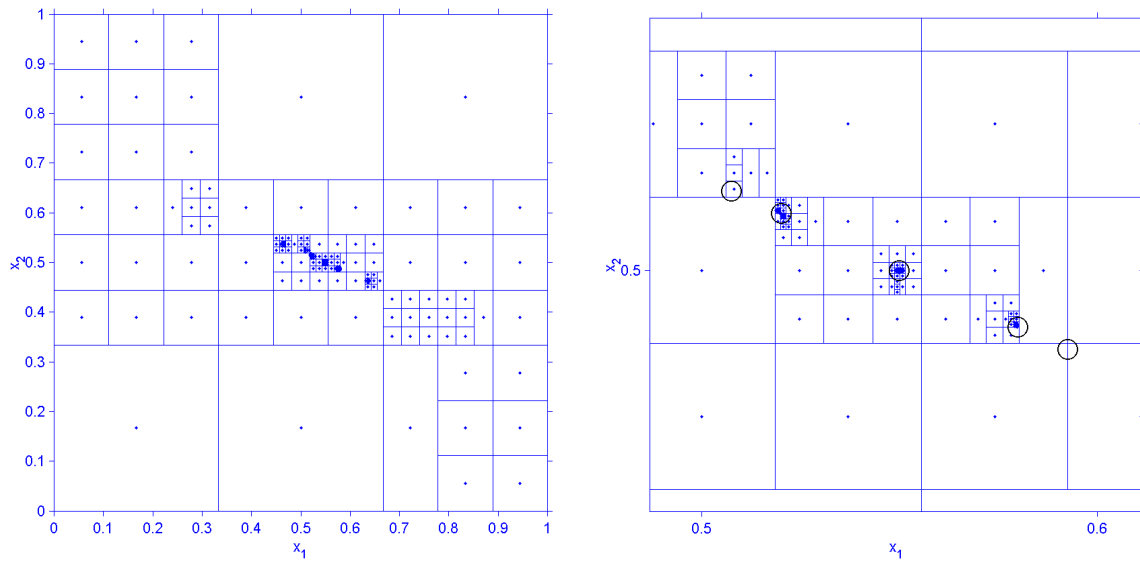


Fig. 57 Results of DIRECT-III + and the local zoom-in

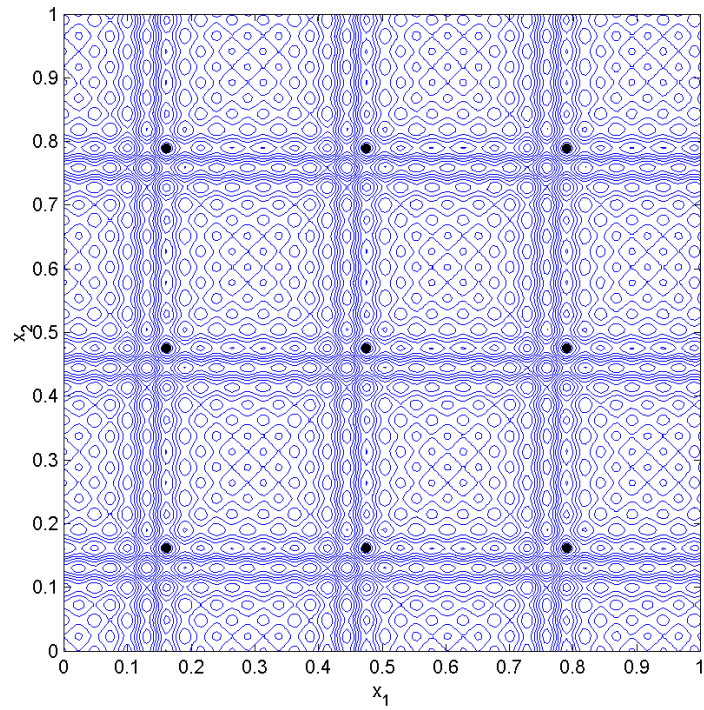


Fig. 58 Contour lines of Shubert function

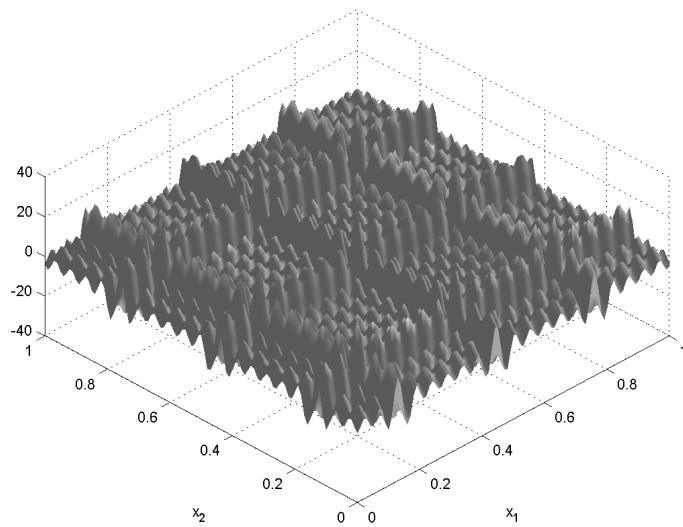


Fig. 59 Surface shape of Shubert function

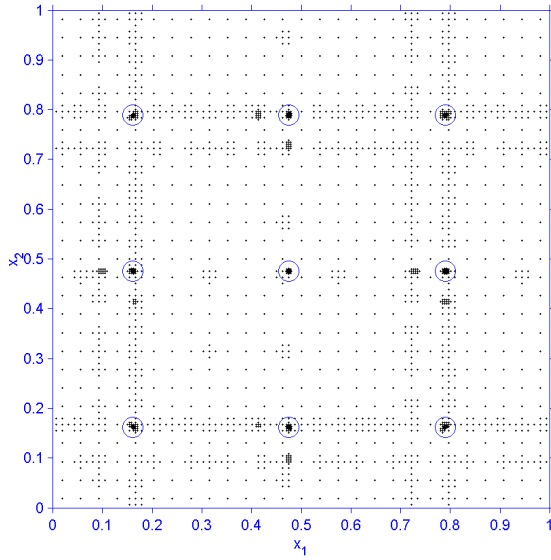


Fig. 60 Results of DIRECT

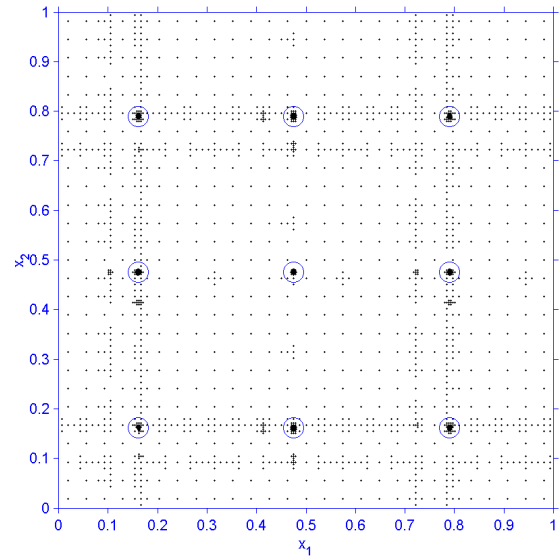


Fig. 61 Results of DIRECT +

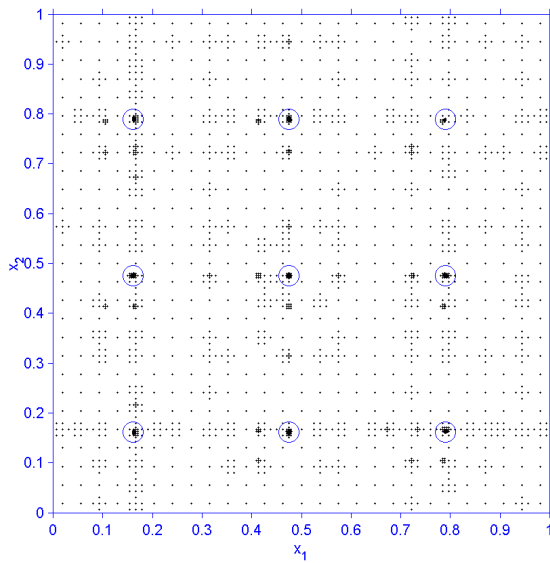


Fig. 62 Results of DIRECT-III

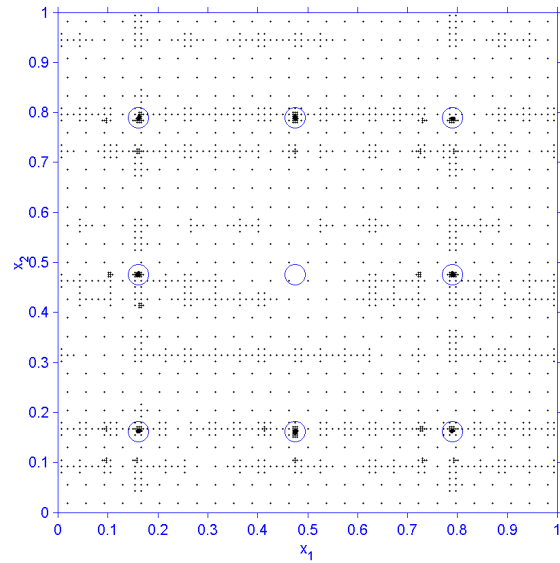


Fig. 63 Results of DIRECT-III +

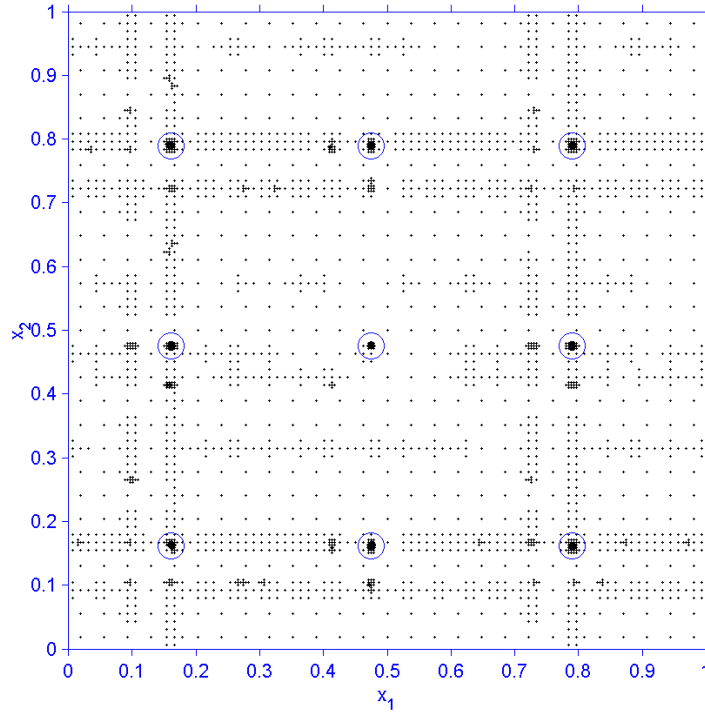


Fig. 64 Results of DIRECT-III + with 4500 function evaluations

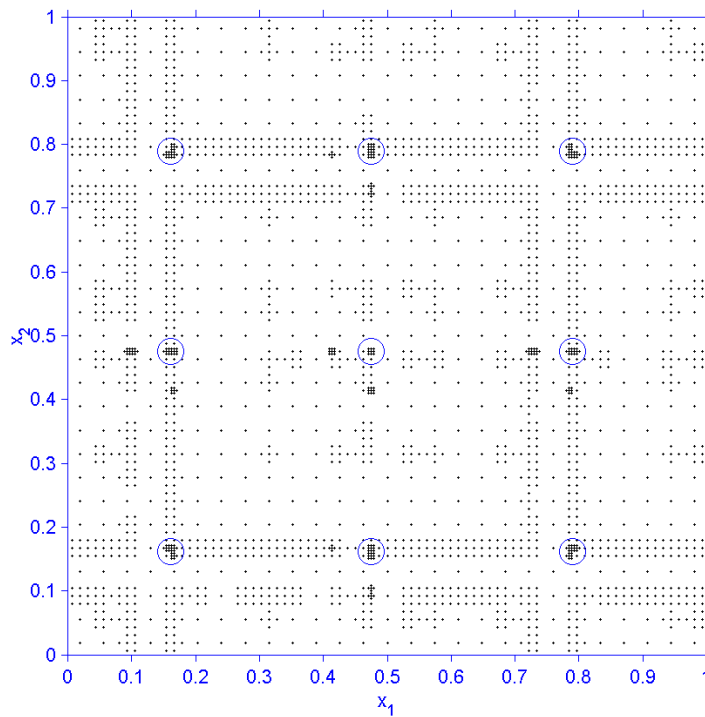


Fig. 65 Results of DIRECT-III + with 0.01 tolerance and 2500 function evaluations

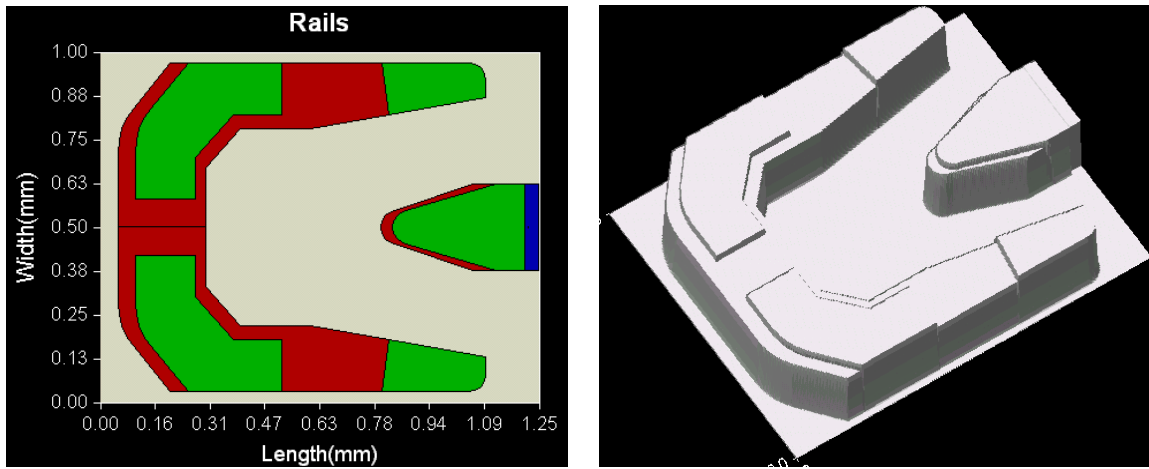


Fig. 66 Rail shape of the initial ABS design Fig. 67 3-D rail geometry of the initial slider

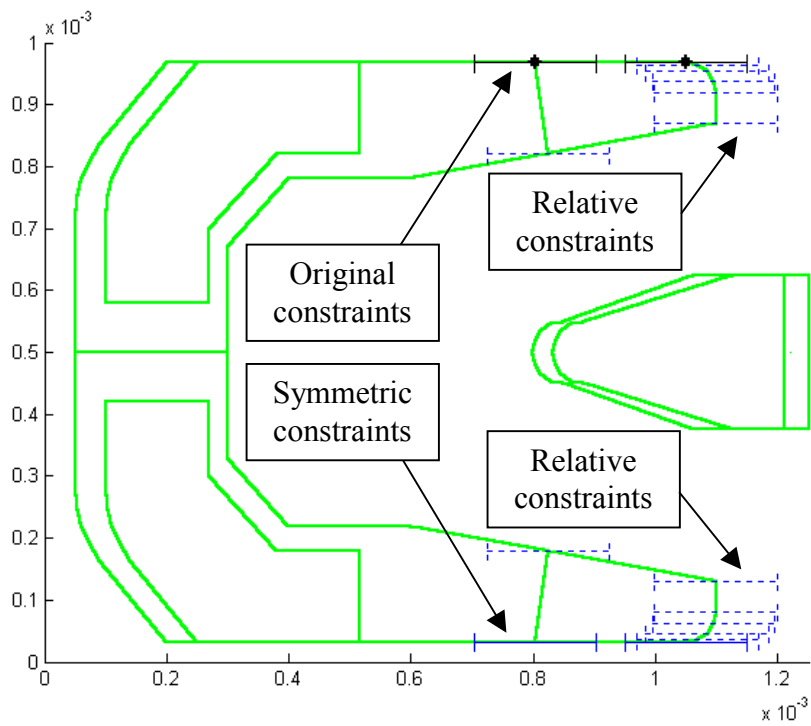


Fig. 68 Constraints defined on the initial design

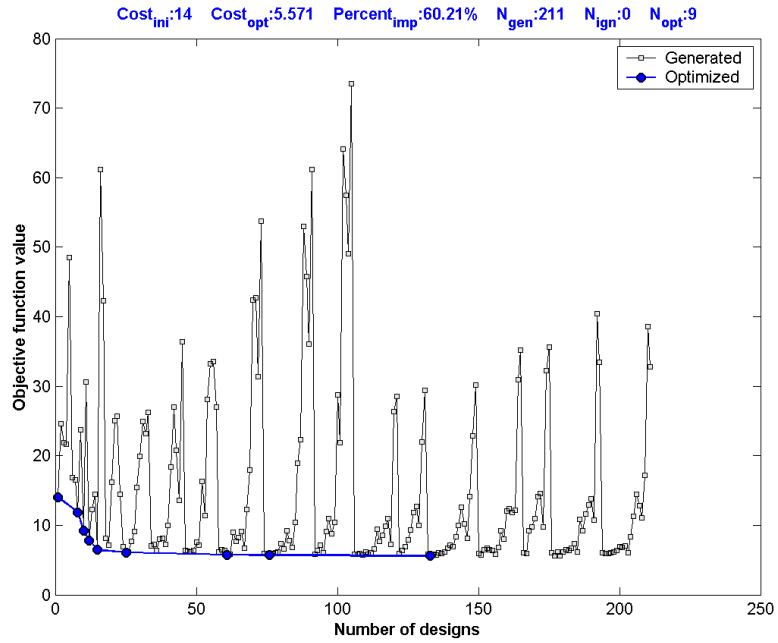


Fig. 69 Variation of the objective function value by DIRECT

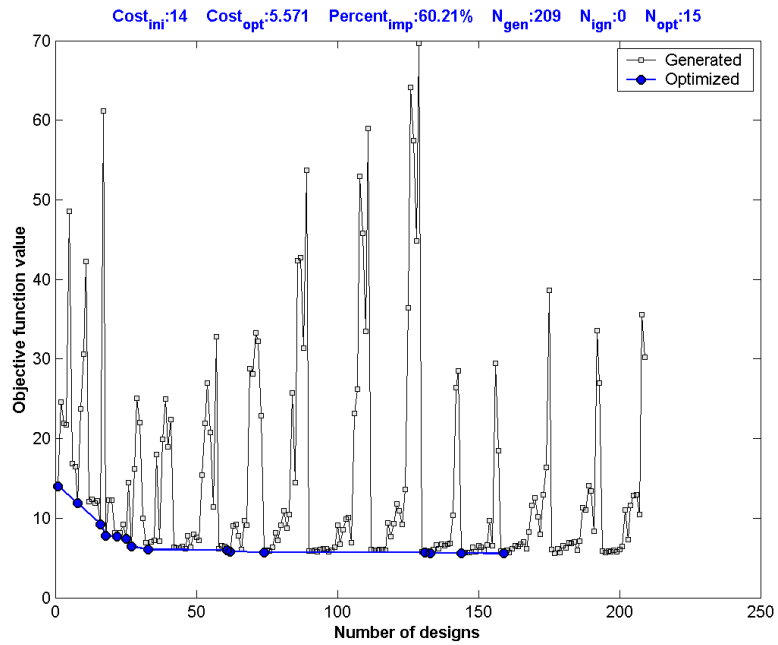


Fig. 70 Variation of the objective function value by DIRECT +

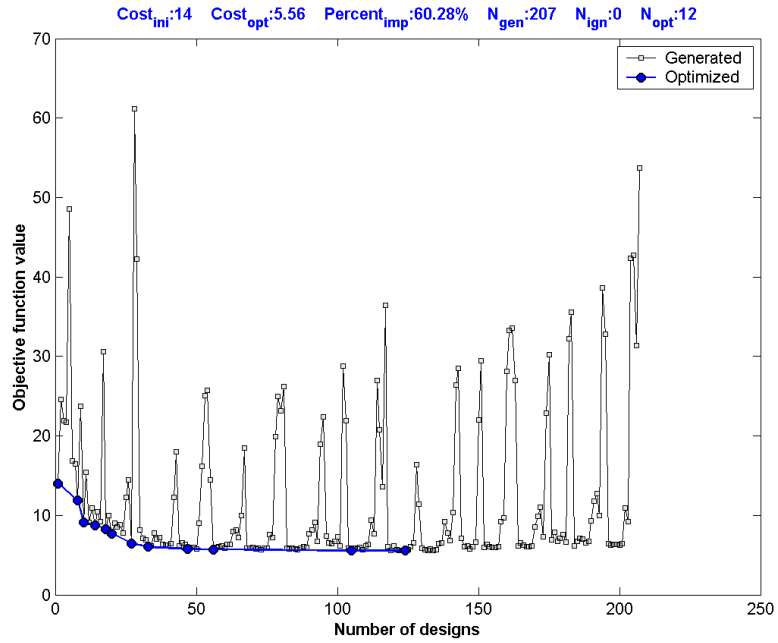


Fig. 71 Variation of the objective function value by DIRECT-III

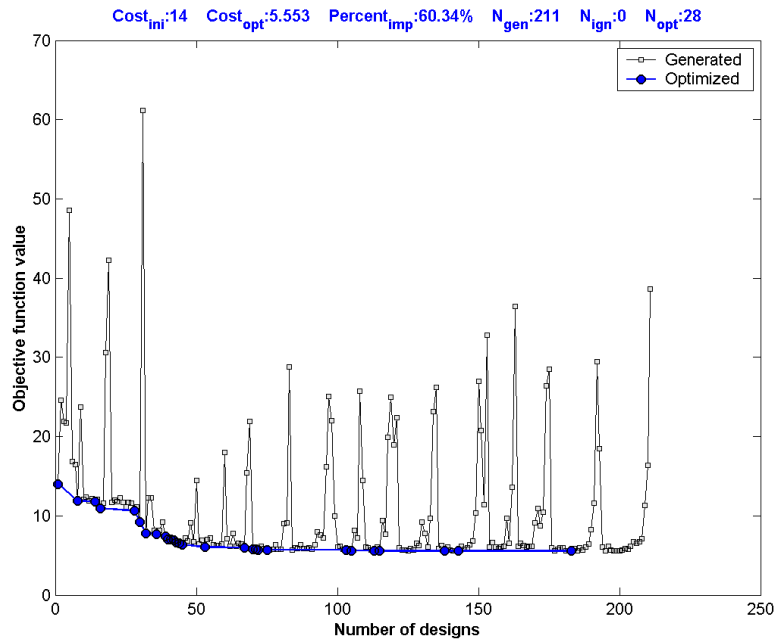


Fig. 72 Variation of the objective function value by DIRECT-III +

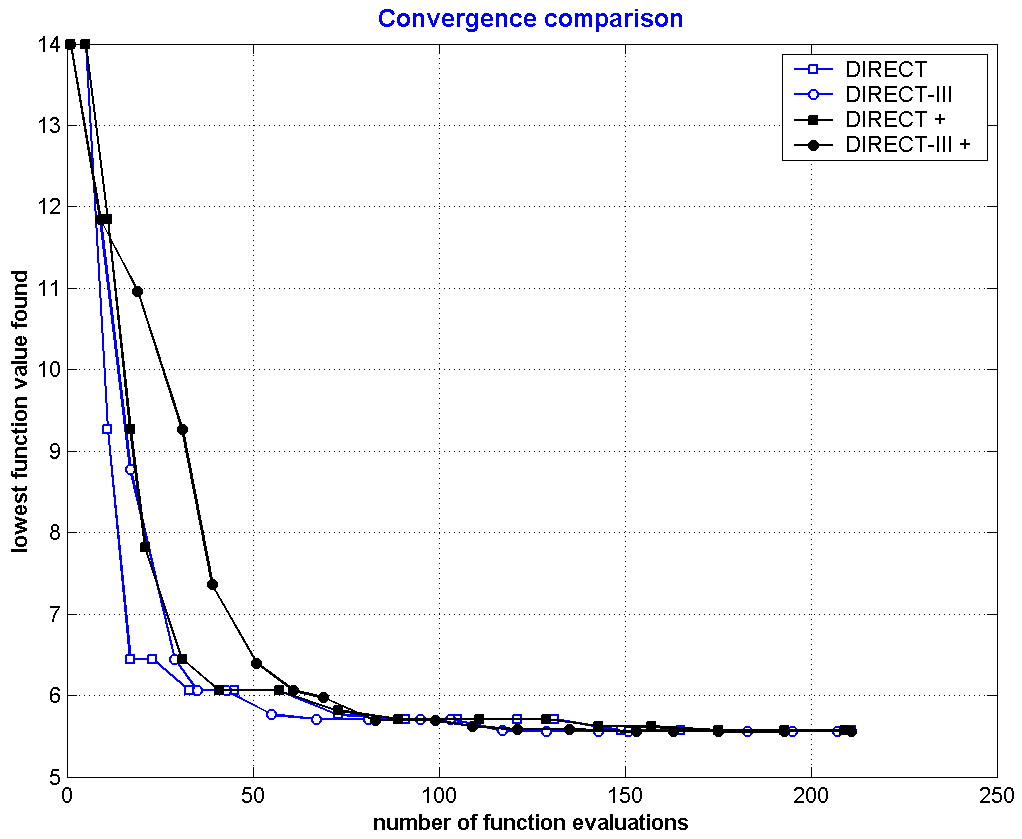


Fig. 73 Convergence comparison for the slider ABS optimization case

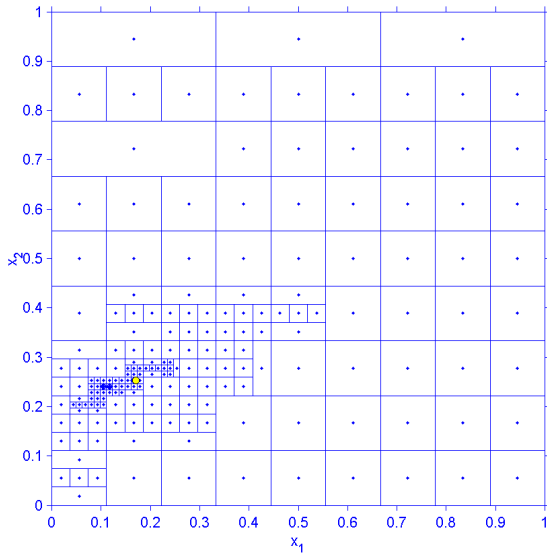


Fig. 74 Results of DIRECT

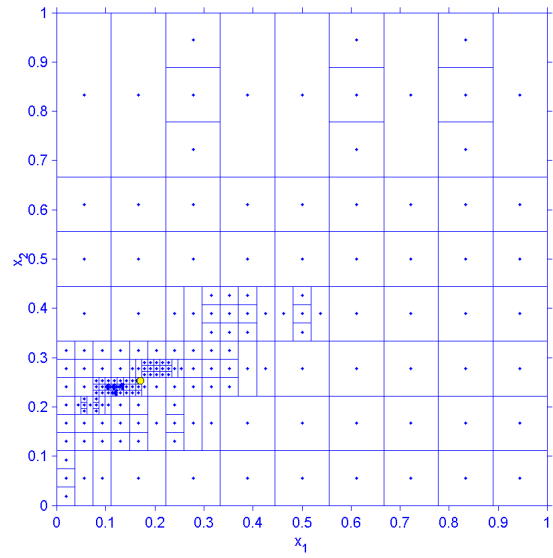


Fig. 75 Results of DIRECT +

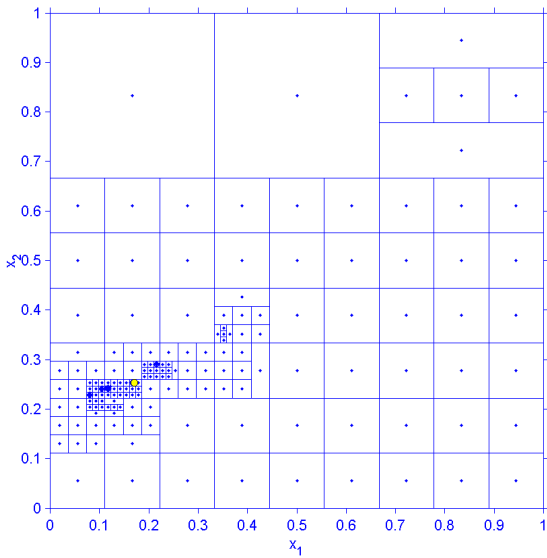


Fig. 76 Results of DIRECT-III

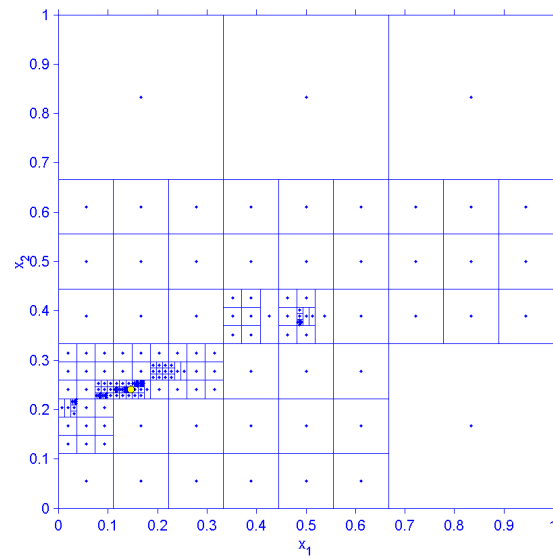


Fig. 77 Results of DIRECT-III +

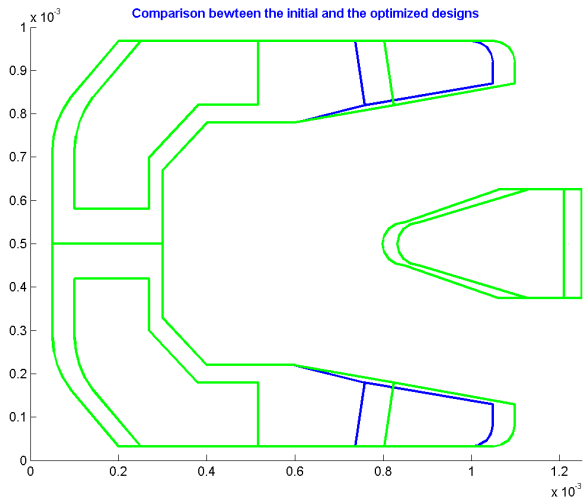


Fig. 78 Optimized ABS design obtained by using DIRECT

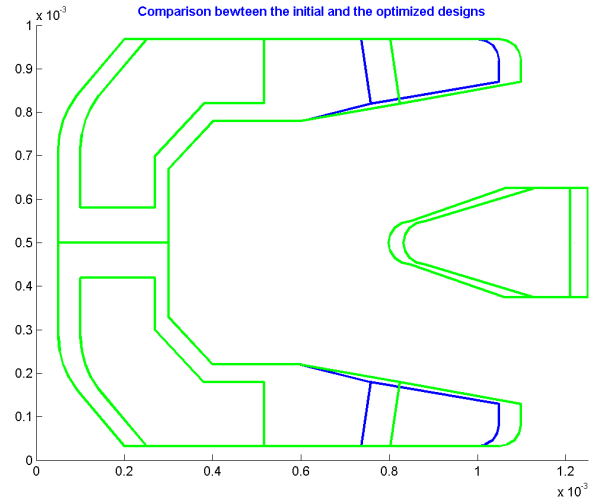


Fig. 79 Optimized ABS design obtained by using DIRECT +

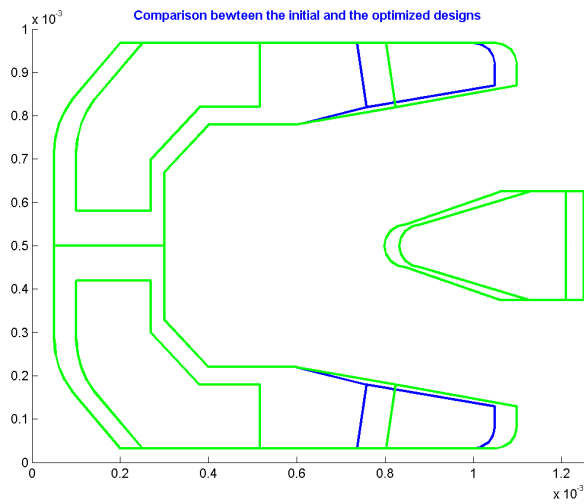


Fig. 80 Optimized ABS design obtained by using DIRECT-III

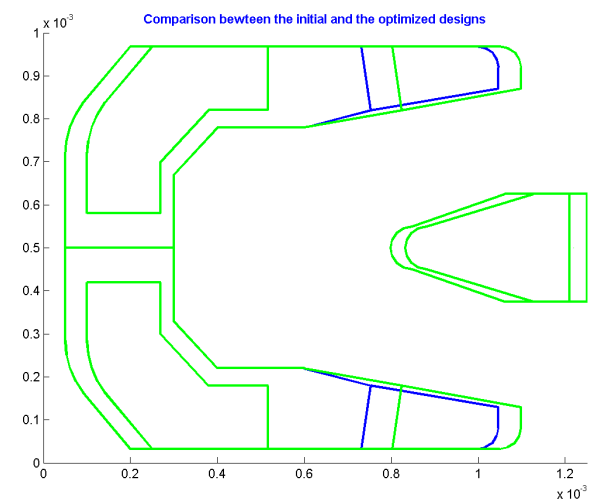


Fig. 81 Optimized ABS design obtained by using DIRECT-III +

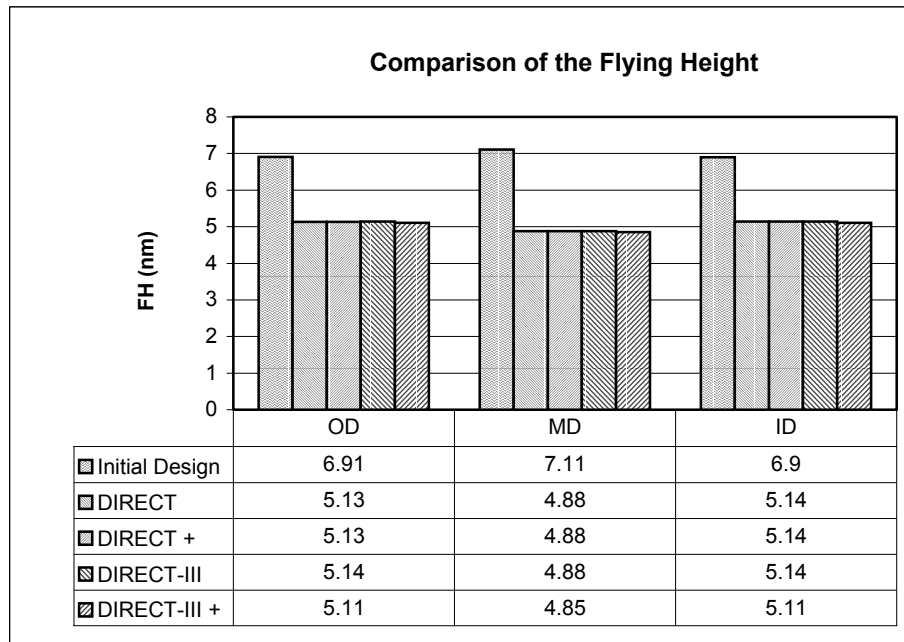


Fig. 82 Comparison of the FH for the slider ABS optimization case

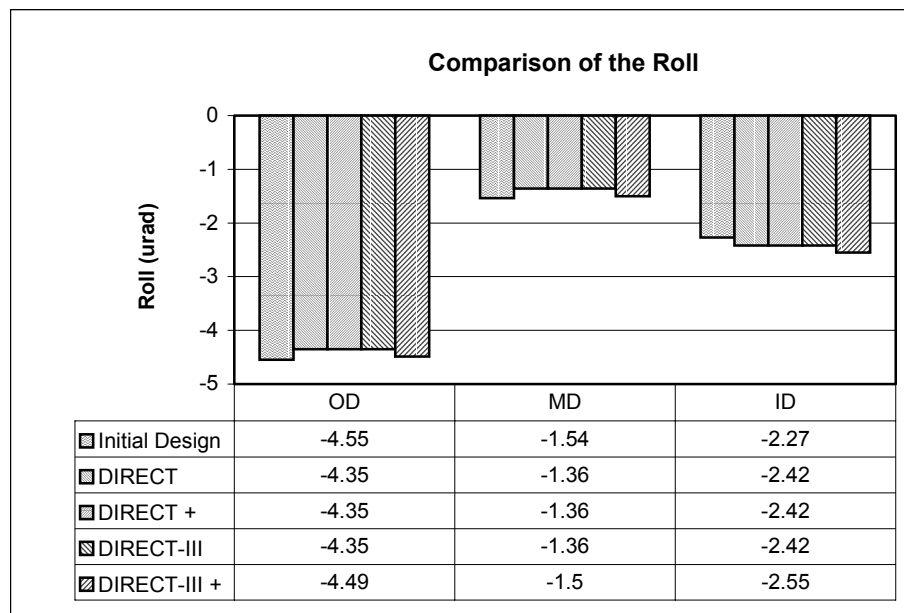


Fig. 83 Comparison of the Roll for the slider ABS optimization case